GEOTHERMAL TRAINING PROGRAMME
Orkustofnun, Grensásvegur 9,
IS-108 Reykjavík, Iceland

Reports 2010
Number 12

MAGNETOTELLURIC AND TRANSIENT ELECTROMAGNETIC METHODS IN GEOTHERMAL EXPLORATION WITH EXAMPLES FROM THE KRÝSUVÍK AREA, SW-ICELAND

Tamrat Fantaye
Geological Survey of Ethiopia (GSE)
Geothermal Resource Exploration and Assessment Core Process
P.O. Box 2302, Addis Ababa
ETHIOPIA
tamuka04@yahoo.com

ABSTRACT

Geophysics plays a great role in subsurface exploration for geothermal resources. Several geophysical exploration methods are applicable, divided into direct and indirect (structural) methods. One of the direct geophysical methods for geothermal exploration is the resistivity method. Electrical resistivity methods like magnetotellurics (MT) and transient electromagnetics (TEM) are powerful tools in mapping subsurface conductivity variations. In this report the main geophysical methods are discussed in general while electromagnetic methods are discussed in detail. MT and TEM data collected along a profile from Krýsuvík high-temperature geothermal area were processed and interpreted and results are presented as resistivity cross-sections. The MT soundings on the profile were aligned in a N-S direction and the corresponding nearby TEM data were analysed for each MT station. 1-D inversion for the TEM data and 1-D joint inversion of MT and TEM data were performed along the profile. The results are presented as resistivity cross-sections. The uppermost layer was found to be resistive, unaltered volcanic rocks while the second corresponds to the conductive smectite-zeolite and mixed layer clay zone. Below these, a relatively resistive layer, corresponding to the chlorite-epidote zone was clearly mapped. The correlation between resistivity values and alteration mineralogy and temperature in wells is also discussed.

1. INTRODUCTION

Geophysics is a science that applies different kind of physical principles to study Earth´s subsurface. Some physical parameters studied are temperature, resistivity, density, magnetization and seismicity. Among these, resistivity and thermal methods are the most successful methods for studying geothermal sites and they are referred to as direct methods. Indirect or structural methods like magnetics, gravity and seismics help to examine the physical parameters of the host rock. Electromagnetic (EM) methods are frequently used in geothermal exploration. This includes magnetotellurics (MT) and time domain electromagnetics (TEM) which are sensitive to resistivity structures beneath. In this report, the main geophysical methods in geothermal exploration, especially EM methods, are discussed and 1-D modelling of MT and TEM soundings from Krýsuvík geothermal field in SW-Iceland is carried out and presented as resistivity cross-sections.

2. GEOPHYSICAL METHODS IN GEOTHERMAL EXPLORATION

Geophysical methods play a key role in geothermal exploration. Different types of geophysical methods are used for geothermal resource exploration. These methods are divided into direct and indirect or structural methods (Hersir and Björnsson, 1991). The former include thermal and electrical methods while the latter include magnetic, gravity and seismic methods.

The most direct method for studying geothermal systems is that of subsurface temperature measurements. Measurements can be made in drillholes as shallow as a few metres or more in the soil, but the preference presently is to conduct temperature surveys in wells that are at least 100 m deep (Manzella, 2007). Thermal methods include direct measurements of temperature or heat and correlate better with the properties of the geothermal system than other methods.

The electrical methods are the most important geophysical methods in the exploration of geothermal systems. This includes direct current (DC) methods and electromagnetic (EM) methods.

DC methods: a constant current is injected into the ground that creates a potential field that can be measured to infer the subsurface resistivity. Schlumberger soundings, head-on profiling and dipole soundings are all DC geophysical methods.

Electromagnetic (EM) methods: Electromagnetic (EM) sounding methods include natural-field methods (magnetotelluric and audiomagnetotellurics) and controlled-source induction methods, as well as high-frequency radiation techniques such as radar-probing. Because of the depth of the main targets in geothermal exploration, only natural-source and controlled-source methods (time domain electromagnetic) are used (Manzella, 2007). This method is described in detail in Section 4.

The gravity method is a structural method through which subsurface geology is investigated on the basis of variations in the earth's gravitational field due to density contrasts between subsurface rocks. It is possible to locate local masses of greater or lesser density than the surrounding formations and get information from the irregularities in the earth´s field. Gravity data are generally affected by several factors and must be corrected for variations such as instrument drift, latitude, elevation and so on.

Magnetic method, also a structural method, is useful in mapping near surface volcanic rocks that are often of interest in geothermal exploration revealing faults or intrusions, but the power of this method lies in its ability to detect the depth at which the Curie temperature is reached (Manzella, 2007). Curie temperature is the critical temperature at which ferromagnetic materials lose their magnetic susceptibility.

Seismic methods are divided into passive and active. Passive seismic methods are natural micro-earthquakes caused by fracturing, sometimes related to geothermal activities; active seismic methods are based on the timing of artificially-generated pulses of elastic energy propagating through the ground and picked up by electromechanical transducers (geophones) as detectors.

3. RESISTIVITY METHODS IN GEOTHERMAL EXPLORATION

Measuring subsurface electrical resistivity is the most powerful method in geothermal exploration (Hersir and Björnsson, 1991). This is because resistivity is directly related to the properties of interest, such as temperature, alteration, salinity and porosity (permeability) (Hersir and Árnason, 2009).

3.1 Resistivity of rocks

The specific resistivity (ρ) of a material is defined as the electrical resistance (R) between the opposite faces of a material (Figure 1), as given by the following equation:

$$\rho = \frac{RA}{l} \tag{1}$$

where ρ = Specific resistivity of the material (Ωm);
R = Resistance (Ω);
l = Length (m);
A = Cross-sectional area of the conducting material (m^2).

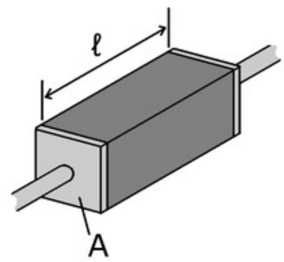

FIGURE 1: A piece of resistive material with electrical contacts on both ends

Electric currents propagate in rocks and minerals in three ways, through electronic (ohmic), electrolytic and dielectric conduction. The first is the normal type of current flow in materials containing free electrons such as metals, while in electrolytic conduction the current is carried by ions at a slower rate. Dielectric conduction takes place in insulators or poor conductors that have no or very few free carriers and conduction takes place by displacement current.

3.2 Factors affecting electrical resistivity of water-bearing rocks

The resistivity of rocks is dependent on and affected by various factors. The rock matrix itself is an insulator and electric conduction occurs through an aqueous solution of common salts distributed throughout the pores of rocks, and through the alteration minerals. The main factors that control the resistivity of rocks are:

- Temperature
- Porosity and permeability
- Salinity
- Water-rock interaction and alteration

3.2.1 Temperature

As shown in Figure 2, at moderate temperatures, 0-200°C, the resistivity of an aqueous solution decreases with increasing temperature. This is because of increasing mobility of the ions caused by a decrease in the viscosity of the electrolytic solution. But at higher temperatures, a decrease in dielectric permittivity of water results in a decrease in the number of dissociated ions in the solution. Above 300°C, this starts to increase the fluid resistivity (Quist and Marshall, 1968).

The relationship between resistivity and temperature of the rock saturated with an electrolyte has been described by Dakhnov (1962) as:

$$\rho_w = \frac{\rho_{wo}}{1 + \alpha(T - T_o)} \tag{2}$$

where ρ_w = Resistivity (Ωm) of the fluid at temperature T;
ρ_{wo} = Resistivity (Ωm) of the fluid at temperature T_o;
α = Temperature coefficient of resistivity, around 0.023/°C for T_o = 23°C, and 0.025/°C for T_o = 0°C.

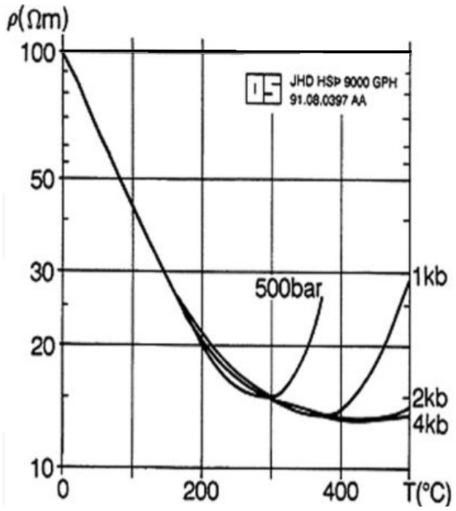

FIGURE 2: Electrical resistivity of aqueous solution as a function of temperature for different pressures (Hersir and Björnsson, 1991)

The effect of temperature variations is greatest at low temperatures (less than 150°C), but decreases at higher temperature when other factors, such as porosity, salinity and alteration mineralogy become dominant (Flóvenz et al., 1985).

3.2.2 Porosity and permeability

The fractional porosity, ϕ_t of a material is defined as the ratio of the pore volume to the total volume of the material and is given by the formula:

$$\phi_t = \frac{V_\varphi}{V} \tag{3}$$

where ϕ_t = Fractional porosity;
V_φ = Volume of voids;
V = Total volume of the material.

Fluid is important for electrical conduction of a rock, therefore the degree of saturation (governed by porosity) is of importance to the bulk resistivity of the rock. The following equation, usually referred to as Archie's law, describes how resistivity depends on porosity if ionic conduction dominates other conduction mechanisms in a rock (Archie, 1942; Hersir and Björnsson, 1991):

$$\rho = \rho_w a \phi_t^{-n} \tag{4}$$

where ρ = Bulk (measured) resistivity (Ωm);
ρ_w = Resistivity of the pore fluid (Ωm);
ϕ_t = Fractional porosity;
α = Empirical parameter that describes the type of porosity varying from <1 for intergranular porosity to >1 for joint porosity, but usually around 1;
n = Cementing factor, an empirical parameter, varies from 1.2 for unconsolidated sediments to 3.5 for crystalline rocks, but usually around 2.

Archie's law is valid if the resistivity of the pore fluid is of the order of 2 Ωm or less, but doubts are raised if the resistivity is much higher (Flóvenz et al., 1985). However, Archie's law seems to be a fairly good approximation when the conductivity is dominated by the saturating fluid (Árnason et al., 2000).

As Figure 3 shows, for pore fluid with resistivity less than 2 Ωm the dominant conductivity is pore fluid conductivity and, hence, Archie's law applies. For rocks saturated with fluids, having resistivity higher than 2 Ωm at room temperature, the bulk resistivity is practically independent of the resistivity of the fluid, but rather dependent on porosity and temperature. The dominant conductivity is mineral and/or surface conductivity.

The permeability of a rock is the ability of fluids to move within its matrix. Permeability depends on the interconnectivity of the pore spaces within the rock matrix. The amount of fluid flowing through a rock can also largely be dictated by fractures (secondary porosity), common in geothermal areas. The wider the fracture, the higher the fracture porosity, hence, high permeability is expressed by the following equation (ISL, Michigan State University, 1999):

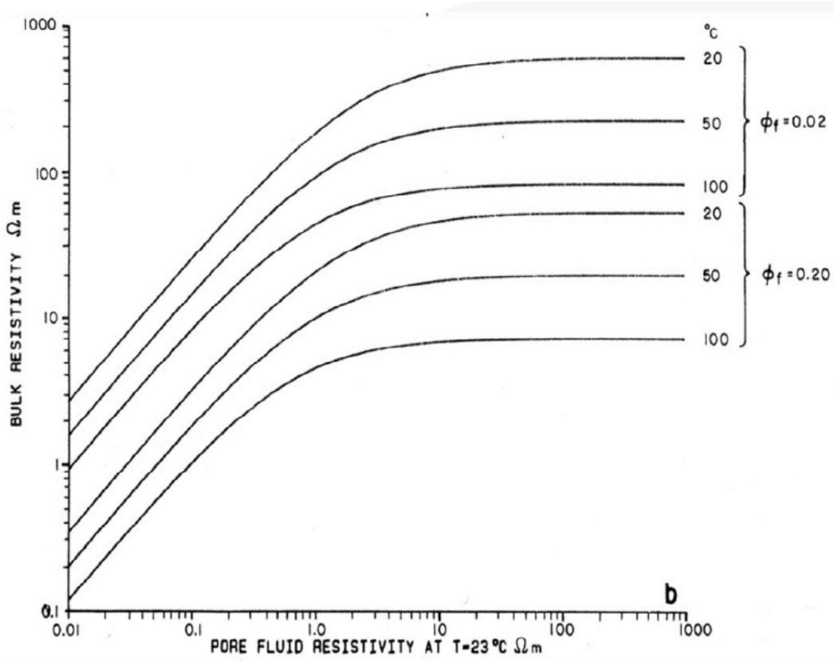

FIGURE 3: Bulk resistivity as a function of pore fluid resistivity for different temperatures and porosities (Flóvenz et al., 1985)

$$K = \frac{Q\eta L}{AP} \tag{5}$$

where K = Permeability (m^2);
Q = Fluid flowrate (m^3/s);
η = Fluid viscosity (kg/ms);
L = Length of the rock (m);
A = Cross-sectional area available for flow (m^2);
P = Pressure drop (Pa)

Geological processes such as faulting, shearing, columnar jointing and weathering usually increase permeability and porosity, thereby increasing electrical conductivity; however, the precipitation of calcium carbonate or silica reduces porosity and, hence, increases resistivity.

3.2.3 Salinity

The conductivity (σ) of a solution depends on the mobility and concentration of the ions present in the solution. This relationship is described by the following equation (Keller and Frischknecht, 1966):

$$\sigma = F(c_1 q_1 m_1 + c_2 q_2 m_2 + \dots) \tag{6}$$

where σ = Conductivity (S/m);
F = Faraday's number (9.65×10^4 C);
c_i = Concentration of ions;
q_i = Valence of ions;
m_i = Mobility of ions.

As shown in Figure 4, when the amount of dissolved ions in the pore fluid increases, conductivity increases. Conduction in a solution is greatly affected by salinity and the mobility of ions present in the solution.

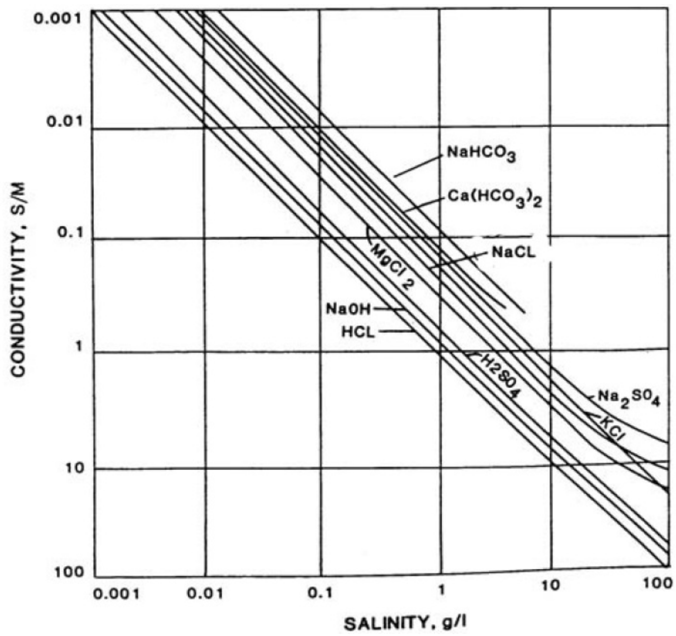

FIGURE 4: Pore fluid conductivity vs. salinity for various electrolytes (modified from Keller and Frischknecht, 1966)

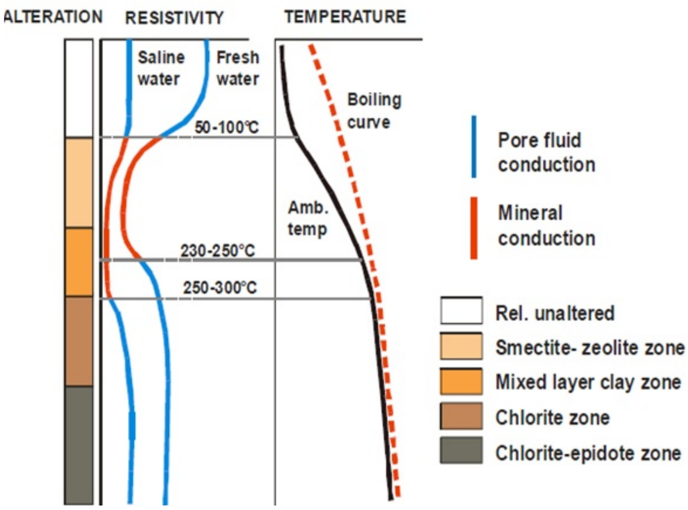

FIGURE 5: A summary of general resistivity structures of high-temperature areas in Iceland (Flóvenz et al., 2005)

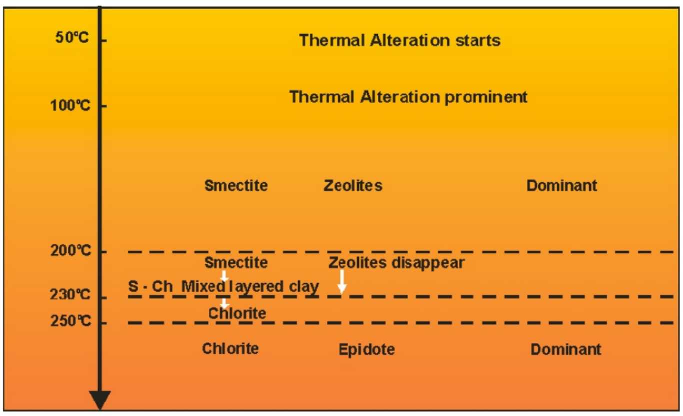

FIGURE 6: Alteration mineralogy and temperature

3.2.4 Water-rock interaction and alteration

The alteration process and the resulting type of alteration minerals are dependent on the type of primary minerals, the chemical composition of the geothermal fluid and temperature. The intensity of the alteration is furthermore dependent on temperature, time and the texture of the host rocks. Alteration intensity is normally low for temperatures below 50°C (Figure 5). At temperatures lower than 220°C, low-temperature zeolites and the clay mineral smectite are formed. Smectite has hydrated and loosely bound cations between the silica plates, making the mineral conductive and with a high cation exchange capacity (Árnason et al., 2000).

In the temperature range from 220 to about 240°C, the zeolites disappear and the smectite is transformed into chlorite in a transition zone, the so-called mixed-layered clay zone, where smectite and chlorite coexist in a mixture (Figure 6). At about 240°C smectite disappears and chlorite is the dominant mineral, marking the beginning of the chlorite zone with increased resistivity, since chlorite minerals have cations that are fixed in a crystal lattice, making the mineral resistive. At still higher temperatures, above 240°C, epidote becomes abundant in the so-called chlorite-epidote zone (Árnason et al., 2000).

4. ELECTROMAGNETIC METHODS

Electromagnetic methods have become powerful geophysical tools in mapping subsurface conductivity variations. The method is widely used in the exploration of geothermal resources (Árnason et al., 2010). It mainly involves the propagation of continuous wave or transient electromagnetic fields in the earth. The source may be natural or artificial. In a natural source method like magnetotellurics (MT), the fluctuation in the earth's natural magnetic field induces an electric field (Figure 7). By measuring the electrical and magnetic field at the surface of the earth, inferences are made about the conductivity distribution in the subsurface.

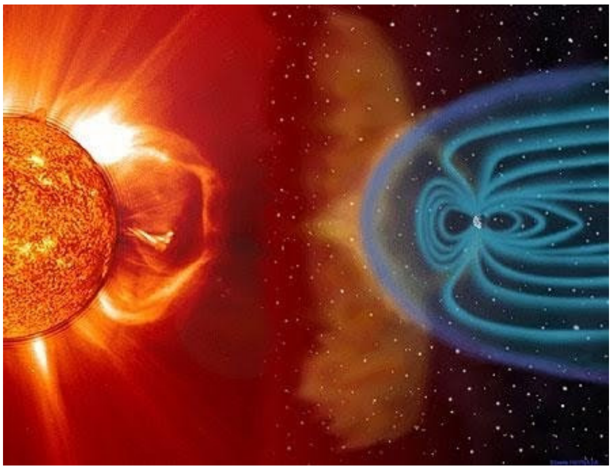

FIGURE 7: Interaction of solar wind with the magnetosphere (SOHO, 2010)

In artificial or controlled source methods like the Transient Electromagnetic Method (TEM), a magnetic field is created by transmitting a current of known magnitude through a loop of wire on the earth's surface and when the current is abruptly turned off, the magnetic field starts to decay with time. This is used to determine subsurface resistivity structures.

In magnetotellurics the presence of near-surface resistivity inhomogeneities can distort the electrical field, since the field is not continuous across a resistivity boundary. This galvanic distortion effect is known as static shift. It shifts the MT apparent resistivity sounding curve (i.e. log ρ_a vs. log T) by some constant scale factor downward or upward. The static shift is a non-inductive change of the MT apparent resistivity response that severely impairs the interpretation of the data. Electromagnetic methods which only measure magnetic fields such as TEM do not have the static shift problems that affect MT soundings (Simpson and Bahr, 2005). Therefore, TEM data can be used in conjunction with MT data from the same or nearby site in order to correct for static shifts (Sternberg et al., 1988). The correction is in such a way that the MT sounding curve is shifted vertically so that the high-frequency part of the MT curve agrees with the TEM curve and consequently, the low frequency MT curve provides an undistorted picture of the deep resistivity section (Jones, 1988).

4.1 Magnetotelluric (MT) method

The MT method is a passive-surface electromagnetic geophysical technique that measures variations in the Earth's natural electromagnetic field to investigate the electrical resistivity structure of the subsurface from depths of tens of metres to tens of kilometres (Vozoff, 1991). The method is passive in the sense that it utilizes naturally occurring geomagnetic variations as the power source. Worldwide lightning activity of frequencies from 10,000 to 1 Hertz (Hz) and geomagnetic micro-pulsations of frequencies from 1 to 0.001 Hz provide the majority of natural signals used by the MT method.

The low frequencies which are less than 1 Hz and originate from solar wind interacting with the earth's magnetic field and ionosphere and are used for deep crustal investigations, while the high frequencies, which originate from thunderstorm activities close to the equator, are used to map resistivity variations of the upper crust. Data acquisition for a single MT station (Figure 8) is done by measuring the input fields, two horizontal magnetic components H_x and H_y and the resulting earth response, two horizontal electrical fields, E_x and E_y and the vertical magnetic field, H_z. The resulting time-series data are recorded and Fourier transformed to the frequency domain for further processing to get the impedance tensors of the apparent resistivity and phase.

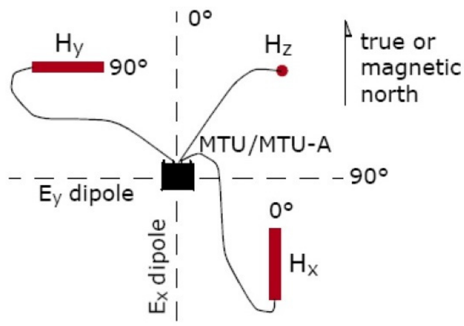

FIGURE 8: Field layout for a 5-channel MT data acquisition system (Phoenix Geophysics, 2009)

For homogeneous earth, when monochromatic electromagnetic plane waves propagate vertically downward, the ratio of the electric to magnetic field intensity is a characteristic measurement of the electromagnetic properties of the medium, often called characteristic impendence (Cagniard, 1953; Keller and Frischknecht, 1966):

$$Z = \frac{i\omega\mu_o}{k} = \frac{E_x}{H_y} = -\frac{E_y}{H_x} \tag{7}$$

where Z = Characteristic impendence;
ω = Angular frequency ($2\pi f$), where f is frequency (Hz);
μ_o = Magnetic permeability in vacuum (H/m);
$E_{x,y}$ = Electric field intensity (V/m) in x, y direction;
$H_{x,y}$ = Magnetic field intensity (A/m) in x, y direction;
k = $\sqrt{i\omega\mu(i\omega\varepsilon + \sigma)}$ is the wave propagation number;
ε = Dielectric permittivity (F/m);
σ = Electrical conductivity (S/m).

For the quasi-stationary approximation, $\sigma >> \omega\varepsilon$, the wave propagation number is approximated to $k = \sqrt{i\omega\mu_0\sigma}$ and Equation 7 can be rewritten as:

$$Z = \frac{i\omega\mu_o}{\sqrt{i\mu_o\sigma\omega}} = \sqrt{i}\,\sqrt{\omega\mu_o\rho} = \sqrt{\omega\mu_o\rho}\,e^{i\pi/4} \tag{8}$$

The phase difference between E_x and H_y is π/4 =45° (Figure 9).

For homogeneous earth, the resistivity is given as:

$$\rho = \frac{1}{\omega\mu_0}|Z|^2\ ;\ Z = \frac{E_x}{H_y} \tag{9}$$

E (V/m) is the electric field and the practical units are mV/km and for the magnetic field ***B*** and magnetic field intensity or magnetization field ***H*** we have $\boldsymbol{B} = \mu_o\boldsymbol{H}$, where $\mu_o = 4\pi\times10^{-7}$ and the practical unit is gamma (1 gamma = 10^{-9} T). Imposing these practical units of E and B to Equation 9 gives:

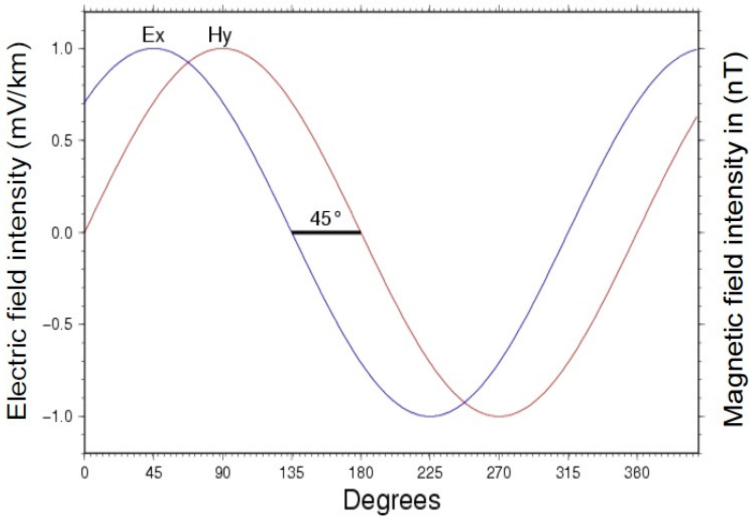

FIGURE 9: Homogeneous half-space response of electric and magnetic field intensity

$$\rho = \frac{T}{2\pi\mu_0}\left|\frac{\mu_0 E_x 10^{-6}}{B_y\,10^{-9}}\right|^2 = \frac{T\mu_0}{2\pi}\left|\frac{E_x}{B_y}\right|^2 10^6 = 0.2T|\frac{E_x}{B_y}|^2 \tag{10}$$

where ρ = Resistivity (Ωm);
T = Period (s)

And for a non-homogeneous earth, we define the apparent resistivity (ρ_a) and the phase (θ_a) as:

$$\rho_a = \frac{T}{2\pi\mu_0}\left|\frac{\mu_o E_x 10^{-6}}{B_y\,10^{-9}}\right|^2 = \frac{T\mu_0}{2\pi}\left|\frac{E_x}{B_y}\right|^2 10^6 = 0.2T|\frac{E_x}{B_y}|^2$$

$$\rho_a = 0.2T|Z_o|^2 \quad and \quad \theta_a = \arg(Z_o) \neq 45° \tag{11}$$

where Z_o = Impedance at the surface.

For horizontally N-layered earth (Figure 10), the plane wave impedance is given by the recursive formula (Ward and Wannamaker, 1983) as:

$$\hat{Z}_N = \frac{\omega\mu_0}{k_N} \; ; \; \hat{Z}_{n-1} = Z_{n-1}\frac{\hat{Z} + Z_{n-1}\, tanh\,(ik_{n-1}h_{n-1})}{Z_{n-1} + \hat{Z}\, tanh\,(ik_{n-1}h_{n-1})} \tag{12}$$

where Z_n $= \frac{\omega\mu_0}{k_n}$ (intrinsic impedance of the n^{th} layer);
k_n $= \sqrt{-(i\omega\mu_0\sigma_n)}$;
h_n = Thickness of the n^{th} layer;
$\hat{Z}_n$ = Impedance in the n^{th} layer;
Z_1 = Z_o is impedance at the surface.

For a two layered earth (Figure 11) where layer one has resistivity ρ_1 and layer two has resistivity ρ_2, Equation 12 becomes:

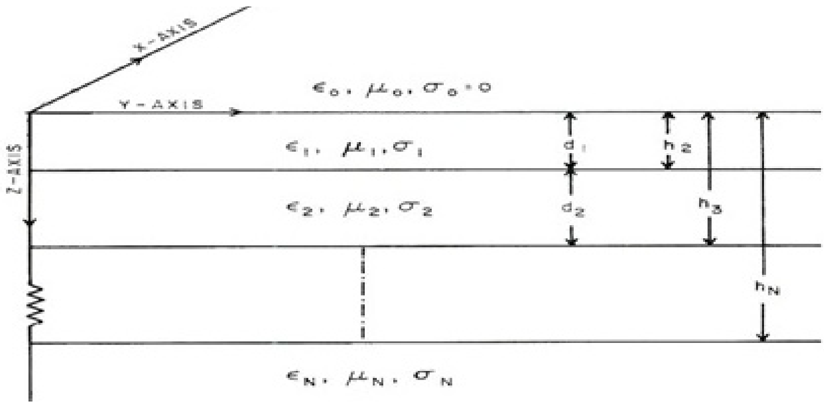

FIGURE 10: *N*-layered earth

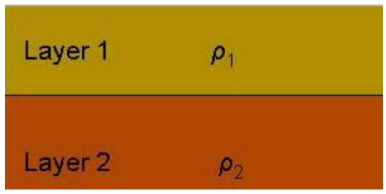

FIGURE 11: Two-layered earth

$$\hat{Z}_1 = Z_1\frac{\hat{Z}_2 + Z_1 tanh\,(ik_1h_1)}{Z_1 + \hat{Z}_2\, tanh(ik_1h_1)} \tag{13}$$

where Z_1 = Z_o = The impedance at the surface; and

$$k_1 = \sqrt{\frac{-i\omega\mu_0}{\rho_1}} = \sqrt{\frac{-i2\pi\mu_0}{\rho_1 T}}$$

For large periods, we have $k_1h_1 << 1$ and this implies $\tanh(ik_1h_1) \approx ik_1h_1$ and then Equation 13 becomes:

$$Z_o = Z_1\frac{\hat{Z}_2 + iZ_1k_1h_1}{Z_1 + i\hat{Z}_2k_1h_1} \tag{14}$$

When the second layer at depth h_1 is a good conductor, $\rho_1 >> \rho_2$ and $Z_1 >> \hat{Z}_2$, Equation 14 becomes:

$$Z_o = Z_1\frac{\hat{Z}_2 + iZ_1k_1h_1}{Z_1 + i\hat{Z}_2k_1h_1} \approx iZ_1k_1h_1 = \frac{i\omega\mu_0}{k_1}k_1h_1 = i\omega\mu_0h_1 \tag{15}$$

and

$$\rho_a = \frac{1}{\mu_0\omega}|Z_o|^2 = \frac{1}{\mu_0\omega}(\mu_0\omega h_1)^2 = \frac{2\pi\mu_0h_1^2}{T} \tag{16}$$

Therefore, the depth to the good conductor, h_1, can be calculated as:

$$h_1 = \sqrt{\frac{\rho_a T}{2\pi\mu_0}} \tag{17}$$

When the second layer at depth h_1 is an insulator, we have $\rho_1 << \rho_2$ and $Z_1 << \hat{Z}_2$, and Equation 14 becomes:

$$Z_o = Z_1 \frac{\hat{Z}_2 + iZ_1 k_1 h_1}{Z_1 + i\hat{Z}_2 k_1 h_1} \approx Z_1 \frac{1}{ik_1 h_1} = \frac{\omega\mu_0}{ik_1^2}\frac{1}{h_1} = \frac{1}{\sigma_1 h_1} = \frac{1}{S} \tag{18}$$

where S = Conductance of layer 1.

The apparent resistivity can be rewritten as:

$$\rho_a = \frac{1}{\mu_0\omega}|Z_o|^2 = \frac{1}{\mu_0\omega}\frac{1}{S^2} = \frac{T}{2\pi\mu_0}\frac{1}{S^2} \tag{19}$$

Therefore, the conductance of the uppermost layer can be calculated from ρ_a for long periods as:

$$S = \sqrt{\frac{T}{2\pi\mu_0\rho_a}} \tag{20}$$

The depth of investigation in MT is a function of subsurface resistivity and frequency (or the inverse of the period) of the electromagnetic signals. The penetration depth can be roughly related to the period by the use of the *skin depth*. The skin depth δ (m) at which the electromagnetic field amplitude is reduced to e^{-1} of its original value at the surface is given as:

$$\delta = \frac{1}{Real(k)} = \frac{1}{Re(\sqrt{i\omega\mu_0\sigma})} = \sqrt{\frac{2}{\omega\mu_0\sigma}} = \sqrt{\frac{2T\rho}{2\pi\cdot 4\pi\cdot 10^{-7}}} = \frac{10^3}{\pi}.\ \sqrt{20/8}\ .\ \sqrt{\rho T} \tag{21}$$

$$\delta \approx 0.5\sqrt{\rho T}\ km$$

4.2 The central-loop TEM method

The transient electromagnetic method (TEM) is a time domain method in which a current pulse is transmitted and the decay of the induced magnetic field is measured as a function of time. A transient event is a short-lived burst of energy in a system caused by a sudden change of state.

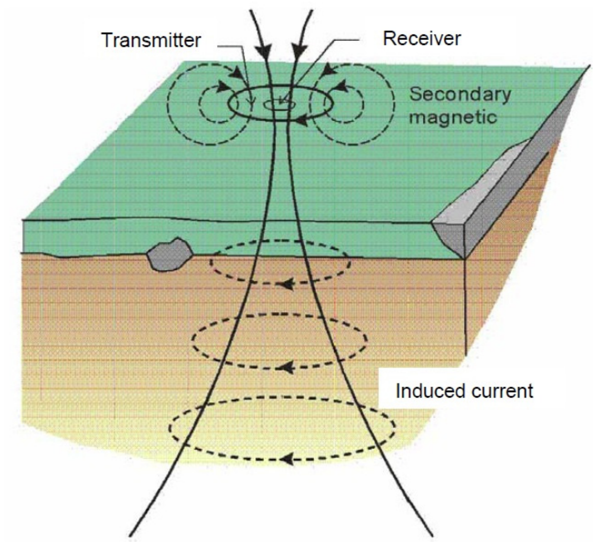

FIGURE 12: Transient current flow in the ground (modified from Hersir and Björnsson, 1991)

Unlike MT, in TEM a current is artificially generated in the ground by a time varying field or a step current transmitted into a loop on the surface. A loop of wire is placed on the ground and a constant magnetic field of known strength is built up by transmitting a constant current into the loop (Figure 12). When the current is turned off abruptly, the magnetic field starts to decay and induces electrical current in the ground. The current distribution in the ground induces a secondary magnetic field decaying with time. The rate of this decay is monitored by measuring the voltage induced in a receiver coil at the centre of the transmitter loop in time gates (Figure 13). The current distribution and the decay rate of the secondary magnetic field depend on the resistivity structure of the earth. The decay rate, recorded as a function of time after the current in the transmitter loop is turned off, can therefore be interpreted in terms of the subsurface resistivity structures (Árnason, 1989).

The primary field impulse (transient) creates eddy currents below the transmitter loop and as the initial near-surface eddy currents decay, they in turn induce eddy currents at greater depths. The rate of change of the secondary field, due to induced eddy currents, is measured using an induction coil. The depth of exploration that will be mapped in a vertical sounding configuration can vary from tens of metres to a thousand metres, depending on the transmitter loop size.

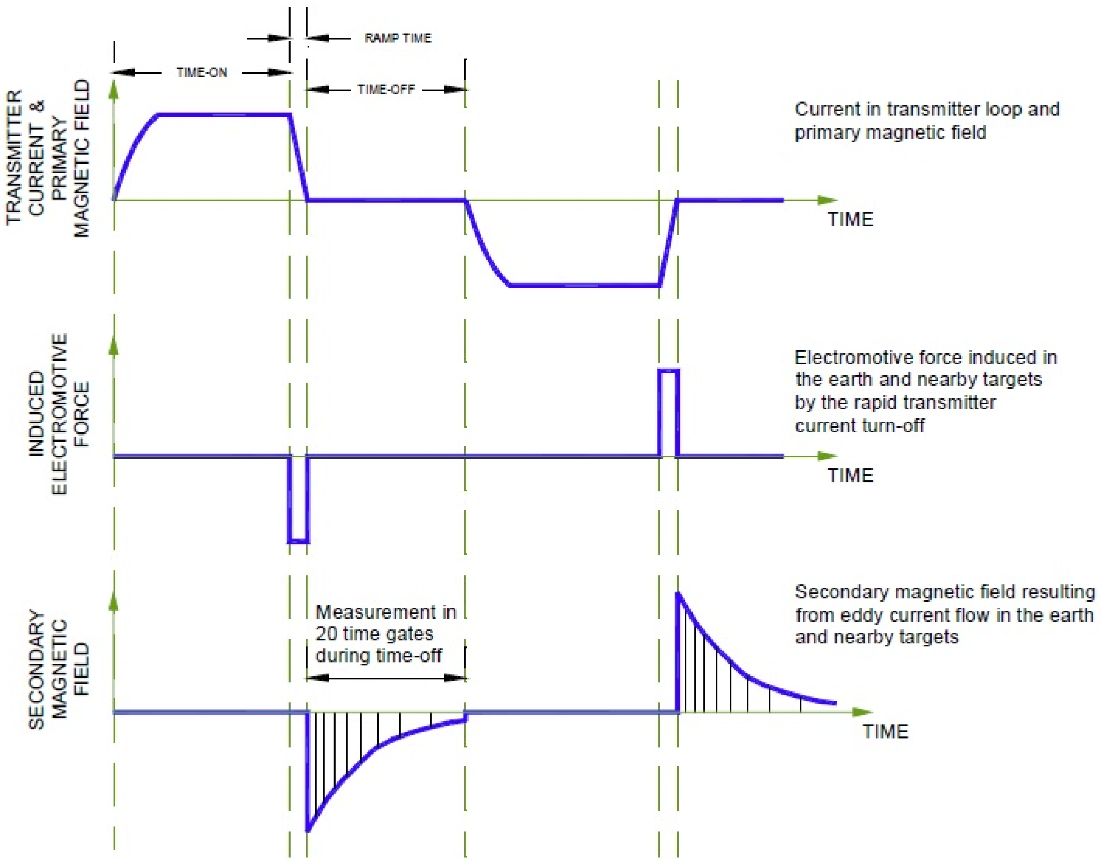

FIGURE 13: Waveforms of the primary and secondary magnetic field (modified from Rowland, 2002)

The basic equation is:

$$V(\omega, r) = A_r n_r A_s n_s I_o e^{i\omega t} \frac{-i\omega\mu}{\pi r} \int_0^\infty \frac{\lambda^2}{m_o} \frac{S_o}{S_o - T_o} J_1(\lambda r)\, d\lambda \tag{22}$$

where A_r = Cross-sectional area of the receiver coil (m^2);
n_r = Number of windings in the receiver coil;
μ = Magnetic permeability (H/m);
A_s = Cross-sectional area of the transmitter loop (m^2)
n_s = Number of windings in the transmitter loop;
r = Radius of transmitter loop (m).

S_o and T_o, which depend on layer resistivity and thickness, are given by the recursion relationships:

$$S_{i-1} = \cosh\ (m_i d_i) - \ T_i \sinh\ (m_i d_i) \tag{23}$$

$$T_{i-1} = -\frac{m_i}{m_{i-1}}[S_i \sinh(m_i d_i) - T_i \cosh\ (m_i d_i)] \tag{24}$$

with $S_{N-1} = 1\ ;\ T_{N-1} = \frac{m_N}{m_{N-1}}$; and

where d_i = The thickness of the i^{th} layer;
m_i = The impedance of the i^{th} layer.

S_o and T_o which determine the voltage (Equation 22) depend on angular frequency, ω and the conductivities σ_i, through $m = \sqrt{\lambda^2 - k_i^2}$ where $k_i^2 = \omega^2 \mu_i \varepsilon_i - i\omega\mu_i\sigma_i$ and ε is the dielectric permittivity. In the quasi-stationary approximation, $\sigma >> \omega\varepsilon$ and hence $k^2 = -i\omega\mu\sigma$.

From Equation 22, the mutual impedance for a central-loop configuration between the source and the receiver coil is defined by the ratio of the measured voltage to the transmitted current as:

$$Z(\omega, r) = \frac{V(\omega, r)}{I_o e^{i\omega t}} = \ A_r n_r A_s n_s \frac{-i\omega\mu}{\pi r}\int_0^\infty \frac{\lambda^2}{m_o}\frac{S_o}{S_o - T_o} J_1(\lambda r)\, d\lambda \tag{25}$$

Equation 22 can be expressed in the time domain by a Fourier expansion of the function describing the transmitted current (Árnason, 1989). If the transmitted current is described by function *I (t)*, a Fourier expansion of the current function will be:

$$I(t) = \frac{1}{(2\pi)^{1/2}}\int_{-\infty}^{\infty} I'\,(\omega)e^{i\omega t} d\omega \tag{26}$$

or

$$I'(\omega) = \frac{1}{(2\pi)^{1/2}}\int_{-\infty}^{\infty} I(t)e^{-i\omega t} dt \tag{27}$$

The induced voltage in the receiver coil in terms of mutual impedance and the Fourier transform of the transmitted current can now be written as:

$$V(t, r) = \frac{1}{(2\pi)^{1/2}}\int_{-\infty}^{\infty} Z\,(\omega, r)I'(\omega)e^{i\omega t} d\omega \tag{28}$$

When the steady current is turned off, the voltage measured as a function of time is given by:

$$V\_(t) = \frac{-I_o}{2\pi}\int_{-\infty}^{\infty}\frac{Z(\omega)}{i\omega}\ e^{i\omega t}\, d\omega = \frac{I_o}{2\pi}\int_{-\infty}^{\infty}\Phi(\omega)e^{i\omega t} d\omega \tag{29}$$

where $\Phi(\omega) = Z(\omega)\ /\!-i\omega$ is a function that depends on ω, its complex conjugate, Φ^* is given as $\Phi^*(-\omega) = \Phi\ (\omega)$.

Therefore, we have:

$$\mathrm{Re}\,\Phi(-\omega) \ = \ \mathrm{Re}\,\Phi(\omega) \ \text{ and } \ \mathrm{Im}\,\Phi(-\omega) \ = \ -\mathrm{Im}\,\Phi(\omega) \tag{30}$$

Therefore, Equation 29 after some calculations becomes:

$$V_{-}(t) = \frac{2I_o}{\pi}\int_0^{\infty} Re\,\Phi(\omega)\cos(\omega t)d\omega = -\frac{2I_o}{\pi}\int_0^{\infty} Im\,\Phi(\omega)\sin(\omega t)d\omega \tag{31}$$

Transient voltage generated in the receiver coil due to a linearly ramped step function is given by (Árnason, 1989):

$$V(t) = \frac{I_o}{TOFF}\int_{-TOFF}^{0} V_{-}(t-\tau)d\tau = \frac{I_o}{TOFF}\int_{t}^{t+TOFF} V_{-}(\tau)d\tau \tag{32}$$

If the current is turned off instantaneously, it would induce infinite voltage in the source loop. Practically, the current is not abruptly turned off but rather in a linear manner in an interval of time called turn-off time (*TOFF*). The turn-off time is measured by the transmitter and fed by the operator into the receiver (Árnason, 2006b).

For a homogeneous half space of conductivity σ, the induced voltage in the receiving coil is approximately given by (Árnason, 1989):

$$V(t,r) = I_o\frac{C(\mu_o\sigma r^2)^{3/2}}{10\pi^{1/2}t^{5/2}}\ ,\ where\ C = A_r n_r A_s n_s\frac{\mu_o}{2\pi r^3} \tag{33}$$

The time behaviour of the diffusing current has three phases: early times, intermediate times and late times. The induced voltage is constant at the early stage and starts to decrease with time in the intermediate stage. At late times, the measured voltage *V(t)* decays in time as $t^{-5/2}$ and varies as $\sigma^{3/2}$ (Árnason, 1989).

Apparent resistivity ρ_a, of a homogeneous half-space in terms of induced voltage at late times after the source current is turned off is given by (Árnason, 1989):

$$\rho_a = \frac{\mu_o}{4\pi}\left[\frac{2\mu_o A_r n_r A_s n_s I_o}{5t^{5/2}V(t,r)}\right]^{\frac{2}{3}} \tag{34}$$

where t = Time elapsed after the transmitter current is turned off (s);
A_r = Cross-sectional area of the receiver coil (m^2);
n_r = Number of windings in the receiver coil;
μ_o = Magnetic permeability in vacuum (H/m);
A_s = Cross-sectional area of the transmitter loop (m^2);
n_s = Number of windings in the transmitter loop;
I_o = Transmitter current (A);
$V(t,r)$ = Measured voltage (V).

5. MT AND TEM SURVEY AT KRÝSUVÍK HIGH-TEMPERATURE GEOTHERMAL FIELD

5.1 Introduction

Krýsuvík is one of the high-temperature geothermal areas in Iceland, located at the centre of the Reykjanes peninsula in SW-Iceland, about 25 km from the capital, Reykjavík (Figure 14). The Krýsuvík high-temperature geothermal field is divided into five sub-fields: Trölladyngja, Hveradalir-Seltún, Austurengjar, Köldunámur and Sandfell.

A total of 96 MT and more than 200 TEM sites have been acquired from the Krýsuvík high-temperature geothermal field and the surrounding area since 1989 and 1-D inverted (Eysteinsson, 1999

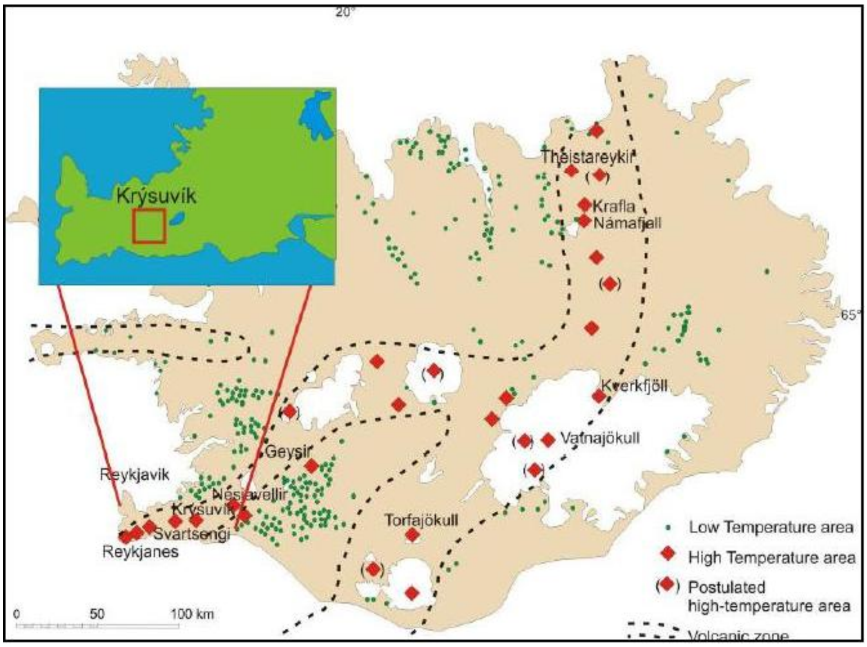

FIGURE 14: Krýsuvík and other geothermal areas in Iceland (map from Ármannsson et al., 2000)

and 2001; Hersir et al., 2010). These data were used in this report with the permission of HS Orka to study the subsurface resistivity distribution of the Krýsuvík high-temperature geothermal field. Multidimensional inversion of the data was done recently by Lemma (2010) as a part of his MSc work. In this study, 11 MT and 11 TEM soundings on a profile were processed and 1-D joint inversion of TEM and MT data was done to correct the static shift. The results are presented as resistivity cross-sections.

5.2 Geologic and tectonic settings of Krýsuvík and surroundings

Krýsuvík is characterised by extensive post-glacial lava fields, steep-sided mountains and ridges of pillow lavas, pillow breccias, and hyaloclastites (Figure 15). It is located at the boundary between an area of predominantly Interglacial eruptions to the east and an area of predominantly sub-glacial eruptions to the west, with formations such as hyaloclastite ridges. The Inter- and Postglacial volcanism, i.e. volcanic activity during the ice free periods, is represented by sub-aerial volcanic products and morphological landscape like explosion craters and lava flows. The common products are lava flows, pyroclastic scoria, welded lava and scoria and explosion breccias.

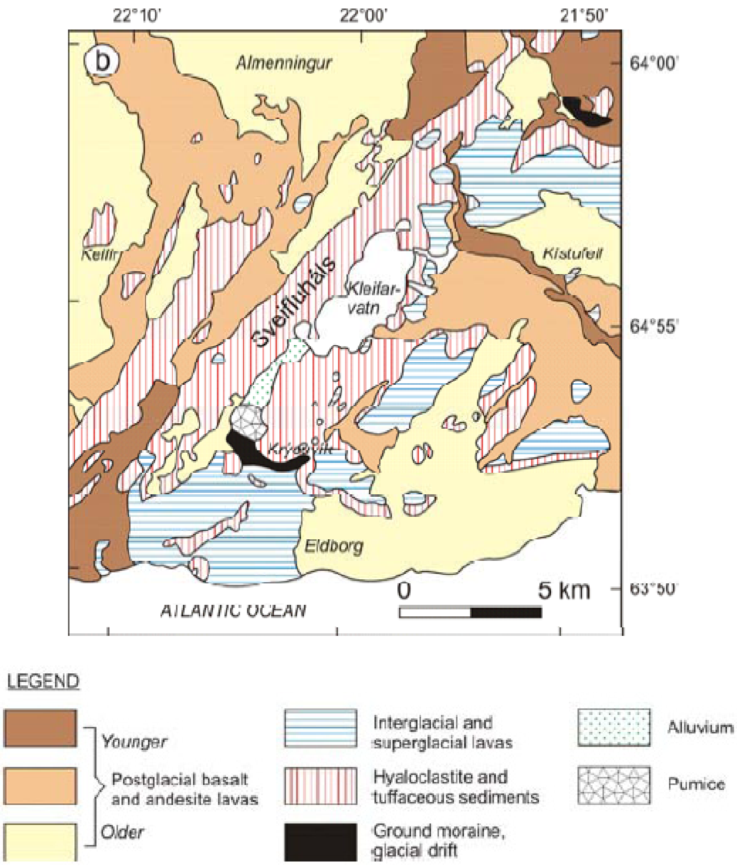

FIGURE 15: Regional geological map of Krýsuvík and surrounding area (taken from Abdelghafoor, 2007)

Krýsuvík lies in a NE-SW elongated valley within the active volcanic zone characterised by fissure swarms striking NE-SW. The Krýsuvík fissure swarm is one of the large en-echelon structural units (fissure swarms) of the Reykjanes Peninsula. Different kinds of surface manifestations observed in the Krýsuvík geothermal system include:

a clay alteration zone, boiling springs, warm springs, mud pools, warm soil, hydrothermal explosion craters and mineralized water in Graenavatn Lake, deposits of silica sinters, oxidation, sulphate deposits, steam vents and mineral veins.

5.3 Instrumentation and data processing

MT instrumentation and field layout: A 5-channel MT data acquisition system (MTU-5) and a 2-channel system (MTU-2EP) from Phoenix Geophysics Ltd were used to record the MT raw data. MTU-5 can acquire two channels of electric field data and three channels of magnetic data from coil sensors. MTU-2EP can acquire two channels of electrical field data. The MTU controls the data acquisition process and converts the signal into a digital format through 24 bit ADU. The instrument synchronizes to Co-ordinate Universal Time (UTC) via signals from the Global Positioning System (GPS) satellites.

A typical layout of a five component MT unit consists of 5 electrodes, 4 of which measure 2-perpendicular horizontal components of the electric field (E_x and E_y), and the fifth electrode is used to ground the MTU data logger at the centre. Out of the 3 induction coils used for magnetic field measurement, 2 of them measure the 2 perpendicular horizontal components (H_x and H_y), and 1 coil measures the vertical component (H_z) of the magnetic field (Figure 16).

FIGURE 16: Phoenix V5 system 2000 hardware components (Phoenix Geophysics, 2009)

Processing and interpretation of MT data: Time-series data downloaded from the MTU-5 unit were viewed using the time series viewer in SSMT2000 program supplied by Phoenix Geophysics Ltd., Canada. The time series viewer is important in analysing the different components of electric and magnetic fields recorded and used to investigate the noisy data (Figure 17). The correlation between E_y with H_x and E_x with H_y is clearly seen on the viewer. The SSMT2000 program takes as input raw time series files, calibration files, and site parameter files. In an intermediate step, it produces Fourier coefficients, which are then reprocessed with data from the reference site, using robust routine processing. The output is MT plot files (.MTH and .MTL) containing multiple cross powers and auto

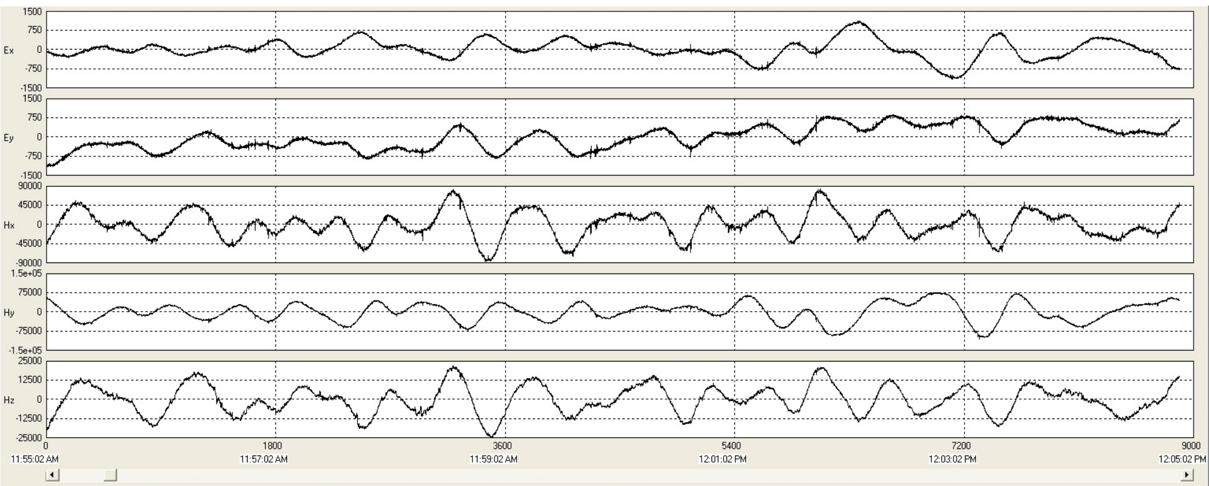

FIGURE 17: Time-series view of a 5-channel MT site

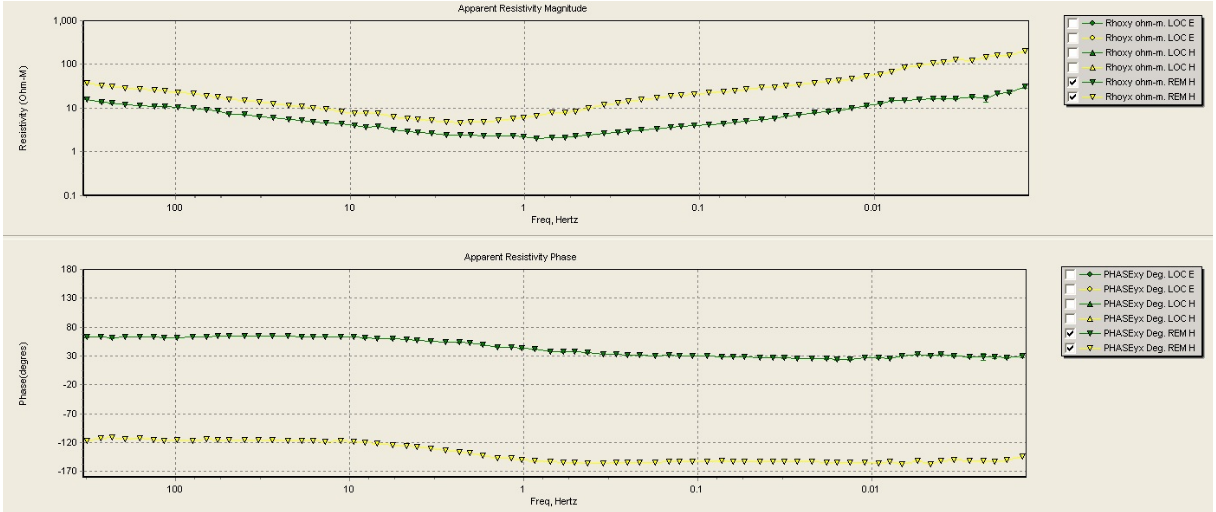

FIGURE 18: MT-Editor output file for MT station 86, showing apparent resistivity and phase curves

powers for each of the frequencies analysed. These MT plot files are used as input in the MT-Editor. The MT-Editor program takes as input the MT plot files created by SSMT2000 and displays the resistivity and phase curves as well as the individual cross powers that are used to calculate each point on the curves. Cross powers that were affected by noise can be automatically or manually masked from the calculations.

The main objective of editing using the MT-Editor is to get a smooth apparent resistivity curve (Figure 18) by eliminating from the calculation of each data point cross powers that were greatly affected by noise. Auto or manual editing can be used according to the data quality; for a normal quality data (low to moderate noise), it is best to start with auto editing and refine the result manually. For very noisy data, it is good to start by deleting all the cross powers for a given frequency and then selectively restoring the best.

The program is also used to display a variety of parameters of the plot files such as tipper magnitude, coherency between channels, and strike direction. After editing was finished, the results were saved as an MPK file and then exported as industry-standard edi (Electrical Data Interchange) files suitable for use with geophysical interpretation programs. The output edi files from MT-Editor were then converted to a UNIX EDI format and a PostScript (ps) file was created to view parameters like apparent resistivity and phase curves (Figure 19). The TEMTD

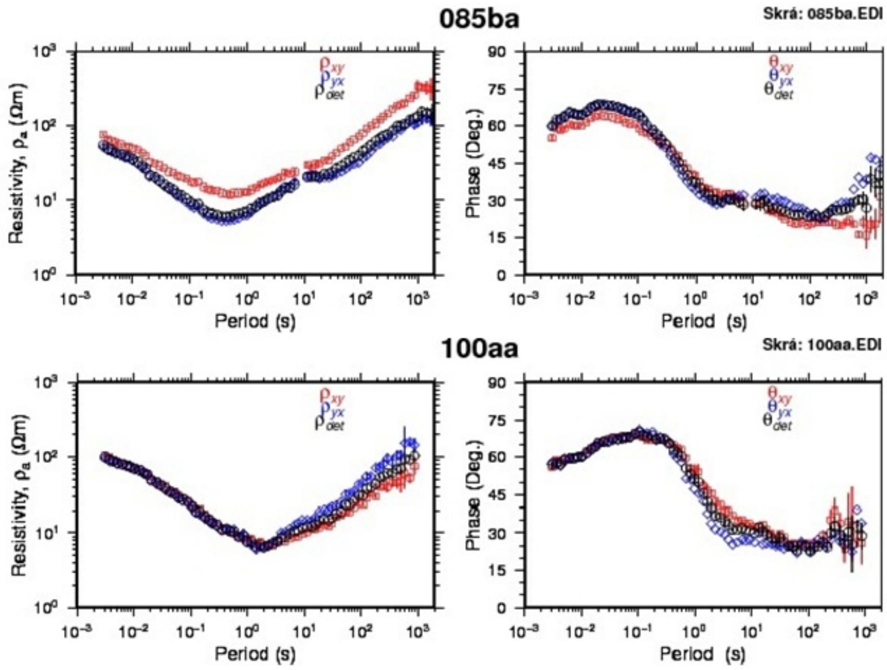

FIGURE 19: Measured apparent resistivity and phase curves from sites 85 and 100 on the profile

program (Árnason, 2006a) was then used to invert the MT soundings (EDI files) jointly with the TEM soundings collected from the same or a nearby site. This joint inversion is important for static shift correction, as discussed in Section 4.

TEM instrumentation and field layout: A time domain electromagnetic equipment, PROTEM-67 from Geonics, Ltd., Canada was used to collect the data. It included a digital receiver, a receiver coil and a square receiver loop, a motor generator, current transmitter and current transmitting loop. The digital receiver and the current transmitter timing are controlled by synchronized high-precision crystal clocks. At each time when the current is turned off, the decay of the secondary magnetic field is monitored by recording the voltage induced in the receiver coil using the digital receiver.

A small receiver coil with an effective area of 100 m^2 and a flexible loop with an effective area of 5613 m^2 were used along with a transmitter square loop of side 300 m. The transmitted current is usually in the range of 20-24 A and data were recorded for both high and low frequencies. The measured induced voltage data were stacked over many cycles and stored in the memory of the data logger together with the corresponding setting information.

Processing and interpretation of TEM data: the raw data downloaded from the PROTEM receiver were viewed and outliers masked using the TemX program from ÍSOR (Árnason, 2006b). The program reads raw data from a PROTEM receiver and calculates the average and standard deviations of the repeated transient voltage and computes late time apparent resistivity. It offers three types of averaging, mean, median value and robust mean that reduce or eliminate outliers. Individual voltage datasets and apparent resistivity for averaged voltage were viewed and noisy readings were masked using the program. After site information was written in the header editing menu, the TemX program produced an output file (.INV), ready for interpretation. An interpretation program from ÍSOR, TEMTD, was used to invert either for voltage or apparent resistivity or both.

TEMTD can be used to invert not only TEM or MT data separately, but also for joint inversion of TEM and MT data where the best static shift multiplier is determined. It uses gnuplot graphics program for graphical display during the inversion process (Figure 20). For TEM data, the program assumes that the source loop is a square loop and that the receiver coil or loop is at the centre of the source loop. The current wave form is assumed to be a half-duty bipolar semi-square wave (equal current-on and current-off segments), with exponential current turn-on and linear current turn-off (Árnason, 2006b). A typical TEM inversion model is shown in Figure 21.

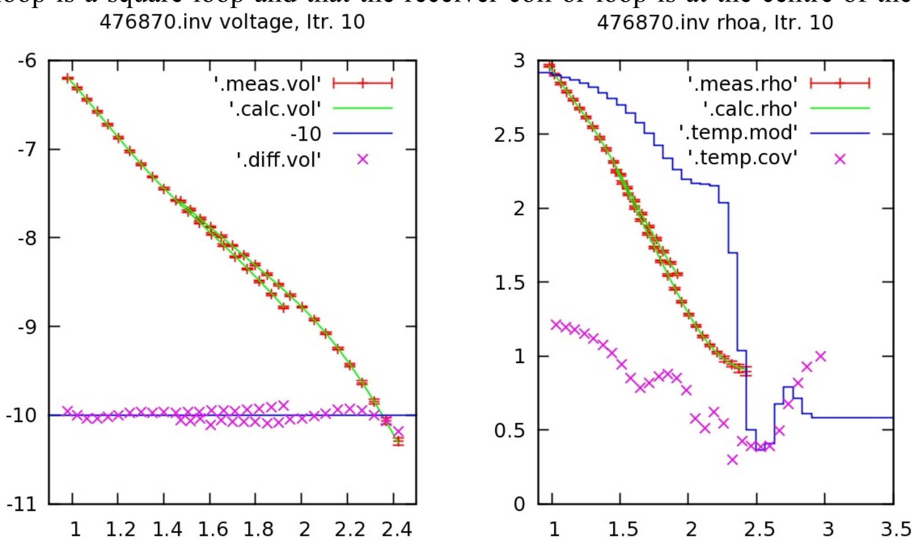

FIGURE 20: TEM data plot during inversion using TEMTD program

The apparent resistivity and phases derived from the determinant of the MT tensor were inverted jointly with the nearby TEM data by this inversion program. As shown in Figure 22, the measured TEM apparent resistivity (red/dark diamonds) curve that overlaps the MT apparent resistivity curve (blue/grey) was used to correct the static shift; the shift multiplier is shown in the upper right corner (0.714). In general, for the 11 stations, the shift multiplier ranged from 0.4-1.3. The response of the resistivity model is shown to the right.

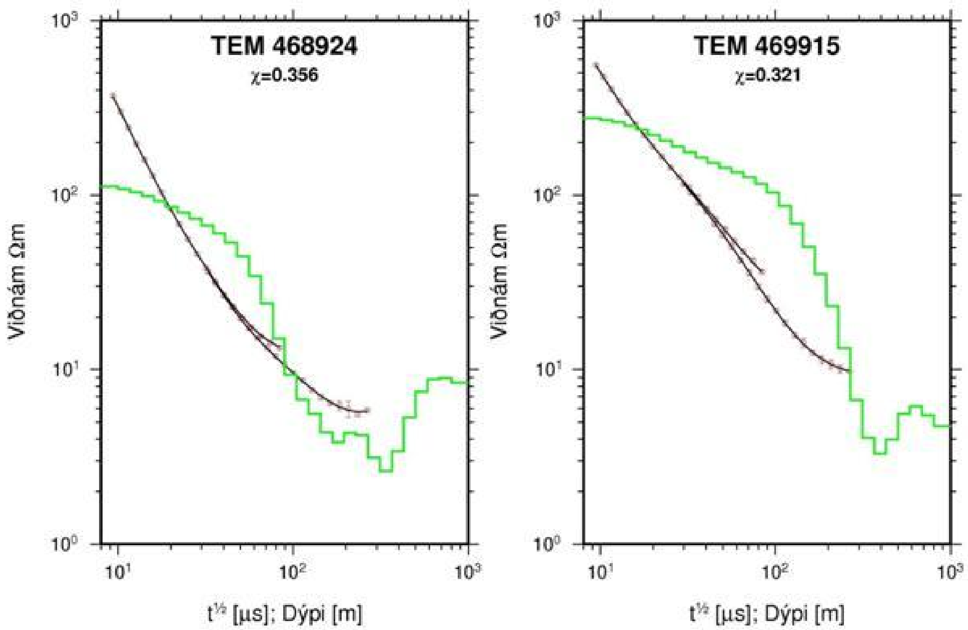

FIGURE 21: TEM inversion model

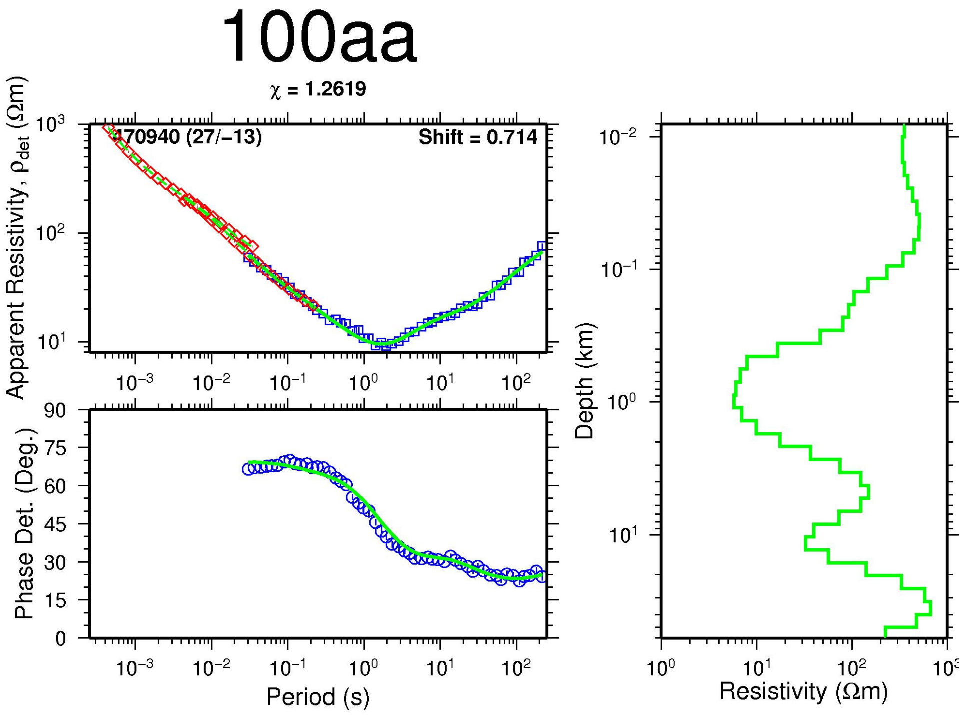

FIGURE 22: Typical result of 1-D joint inversion of TEM and MT soundings

5.4 1-D inversion of resistivity data at Krýsuvík

A total of 11 TEM and 11 MT sites on a profile that crosses the main geological structures of the Krýsuvík high-temperature geothermal field were analysed. The TEM data for the 11 sites was first inverted and interpreted and then jointly inverted with the MT data. The results were used to create resistivity cross-sections by using the TEMCROSS program, written by Dr. Hjálmar Eysteinsson (Eysteinsson, 2010), and the GMT (generic mapping tool) program package. The location of the profile along with main structures and features is shown in Figure 23.

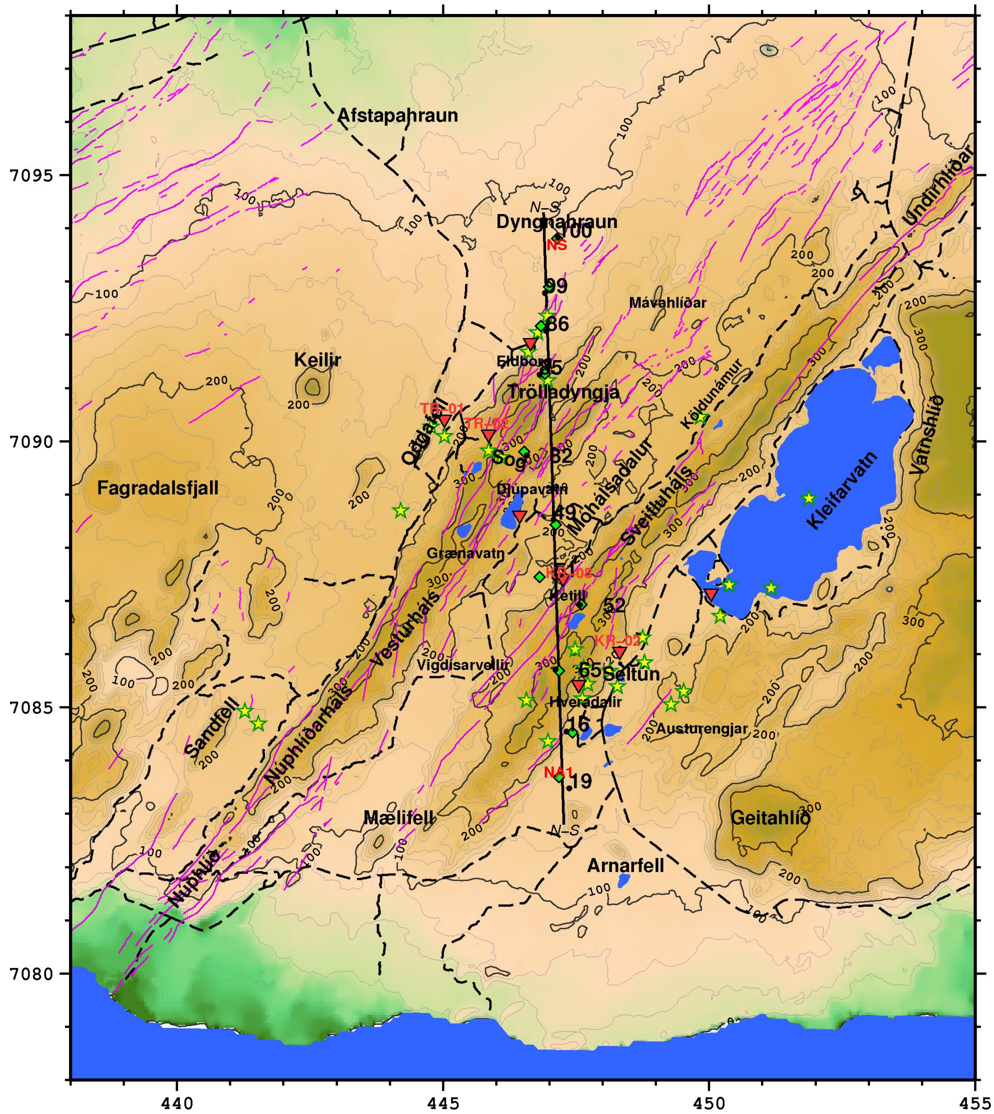

FIGURE 23: Location of the resistivity profile showing: TEM stations (diamonds), MT stations (dots), geothermal wells (inverted triangles), surface manifestations (stars), faults and fissures (scattered lines)

5.4.1 TEM and MT resistivity cross-sections

The TEM resistivity cross-section from 1-D inversion of each sounding on the profile is shown in Figure 24. The resistivity structure, down to a depth of 1000 m b.s.l., was clearly mapped in the TEM cross-section. The inversion model for each TEM station is shown in Appendix I. From the resistivity cross-section, that runs from north to south, it can be seen, that high-resistivity layers with resistivity > 70 Ωm are dominant in the uppermost part of the subsurface. This is due to unaltered volcanic rocks, dry lavas, basalts and hyaloclastites. The presence of water in the subsequent layers decreases the resistivity to a range of 10-100 Ωm. Below these resistive layers, conductive layers or cap with resistivity values of < 10 Ωm were observed. This conductive cap was interpreted as the smectite-zeolite zone that characterises the high-temperature geothermal systems in Iceland (Árnason et al., 2000). The third sequence of layers in this cross-section was a relatively resistive structure that could be related to the chlorite-epidote zone. Correlation with temperature and alteration mineralogy is discussed in Section 5.4.2.

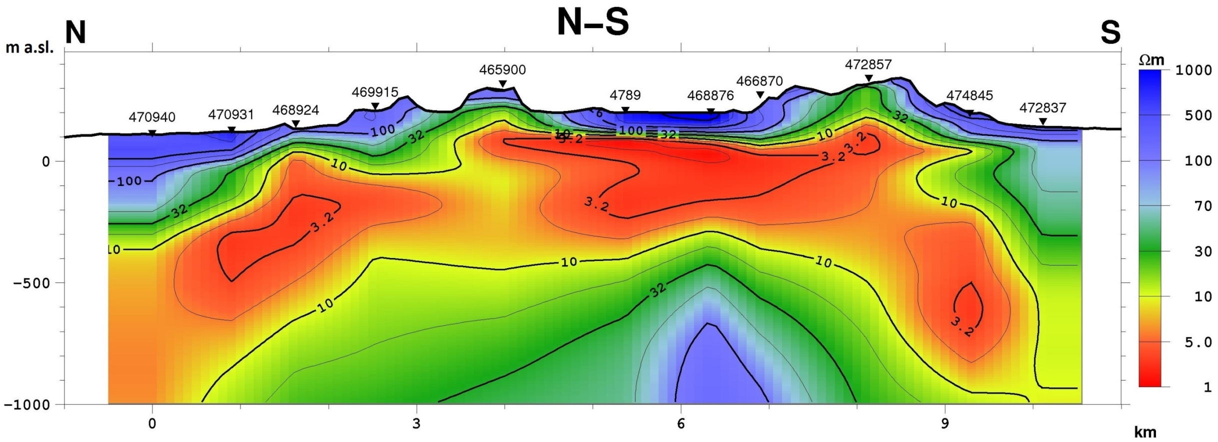

FIGURE 24: TEM resistivity cross-section along the profile down to 1000 m b.s.l.

The results of the joint inversion of the TEM and MT data are presented on the three resistivity cross-sections down to a depth of 2.5, 5 and 20 km as shown in Figures 25, 26 and 27, respectively. The processed MT data are shown in Appendix II, while the joint TEM and MT inversion model for each MT station is shown in Appendix III. It is clearly seen also in these resistivity cross-sections that highly resistive fresh rocks dominate the uppermost layers followed by less resistive layers and then by a conductive cap. This conductive cap formation is characteristic of high-temperature volcanic geothermal field and is associated with the smectite-zeolite or mixed layered clay zone. Below these layers, high-resistivity layers are observed which could be the indication of the high-temperature alteration zone (chlorite-epidote zone). In the resistivity cross-section, which reaches down to a depth of 20 km (Figure 27), a deep laying conductor was observed which can be seen under high-temperature geothermal areas associated with volcanic systems in Iceland (Árnason et al., 2010).

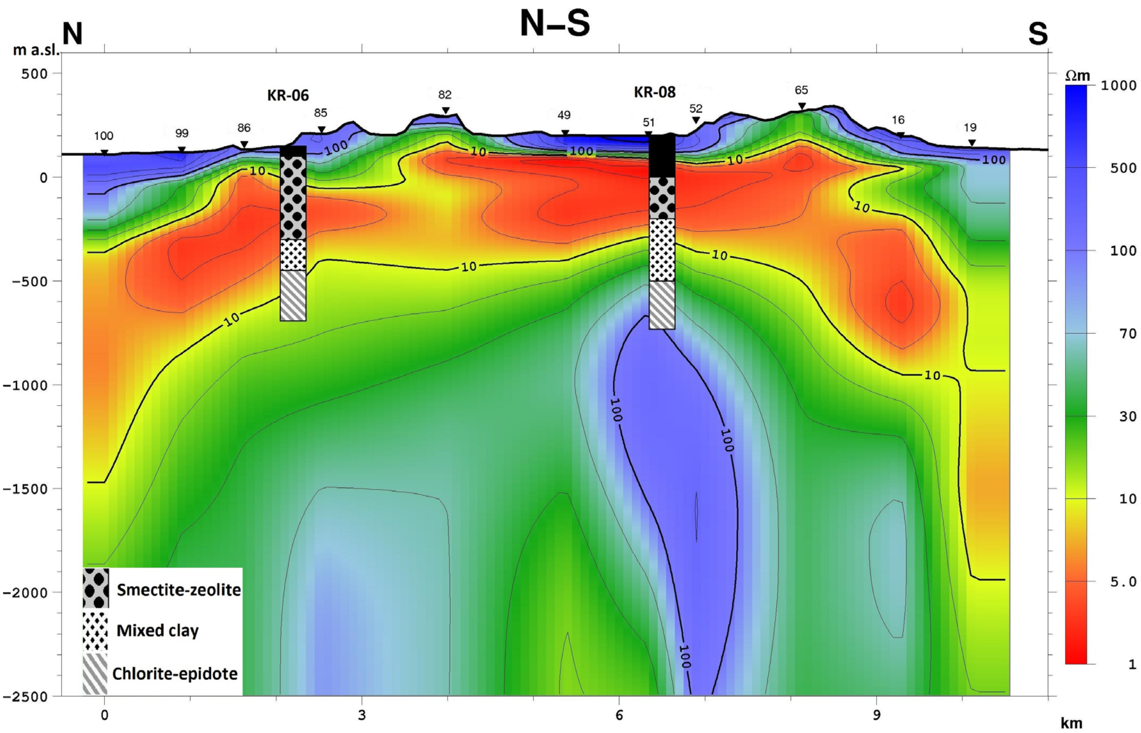

FIGURE 25: Resistivity cross-section from 1-D joint inversion of TEM and MT data down to a depth of 2.5 km b.s.l.

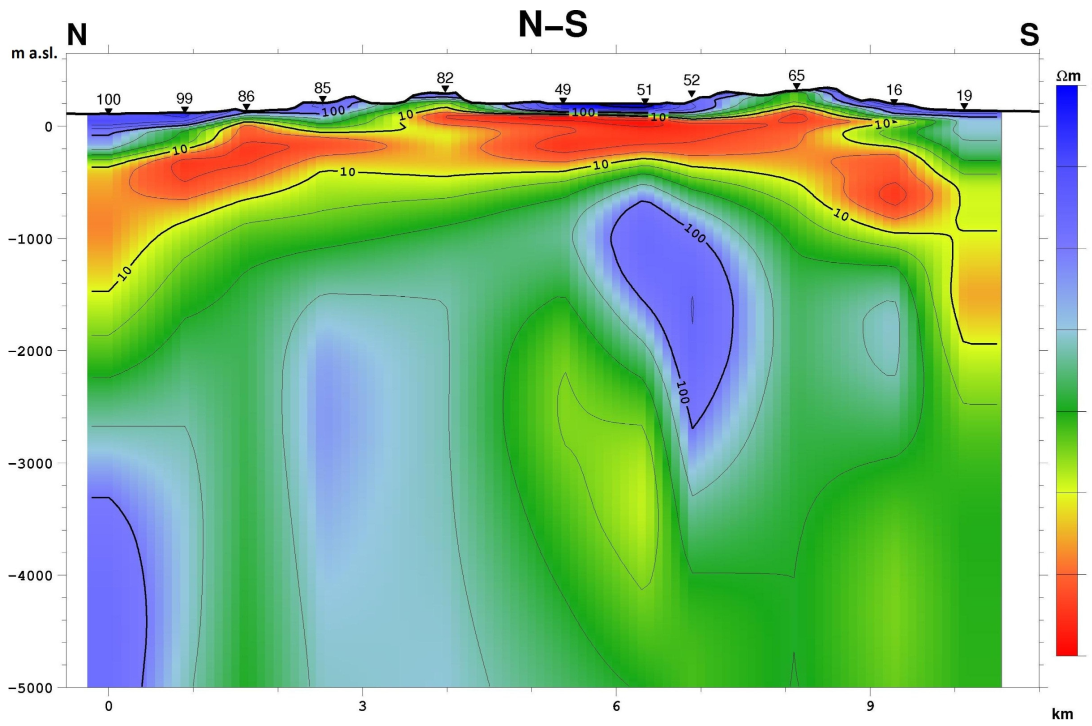

FIGURE 26: Resistivity cross-section from 1-D joint inversion of TEM and MT data down to a depth of 5 km b.s.l.

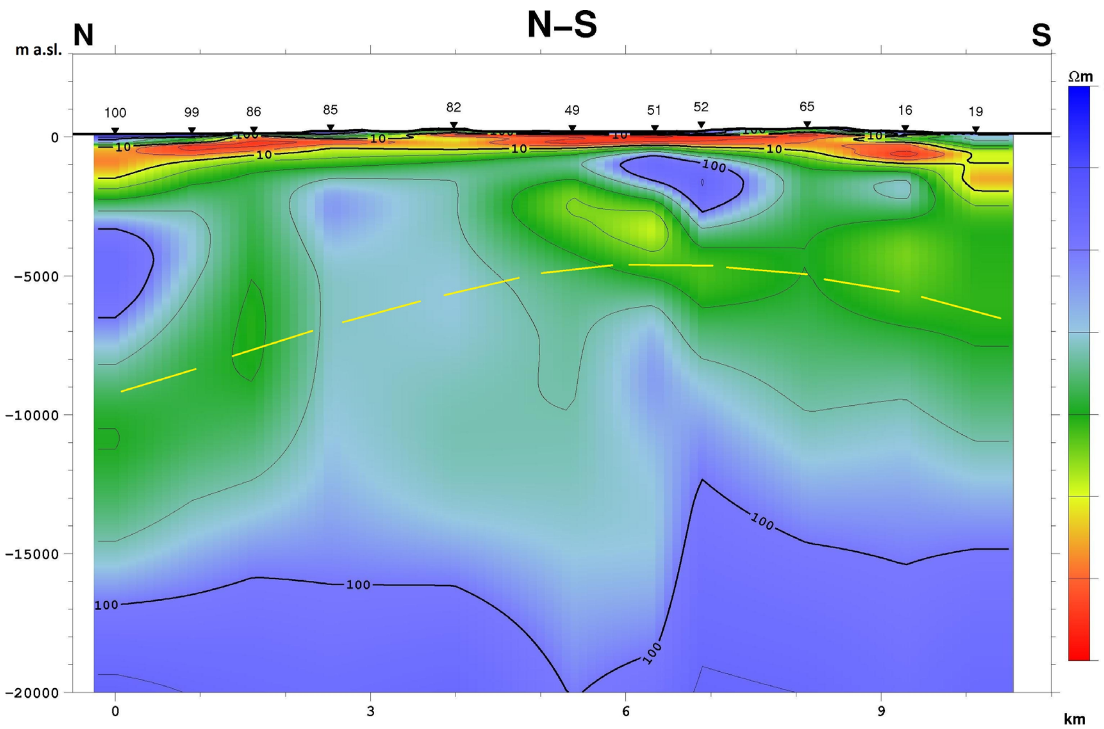

FIGURE 27: Resistivity cross-section from 1-D joint inversion of TEM and MT data down to a depth of 20 km b.s.l.

5.4.2 Alteration mineralogy and temperature in drillholes

The resistivity cross-section along the profile down to 1000 m b.s.l. was compared to the nearby drillhole data from wells KR-06 and KR-08 (Arnórsson et al., 1975), see Figure 25. The minerals observed from the drillhole data include: calcite, laumontite, zeolite, gypsum, smectite, pyrite, mixed clay minerals, epidote and chlorite. These secondary minerals of the basaltic rock are the result of hydrothermal alteration under different pressures and temperatures.

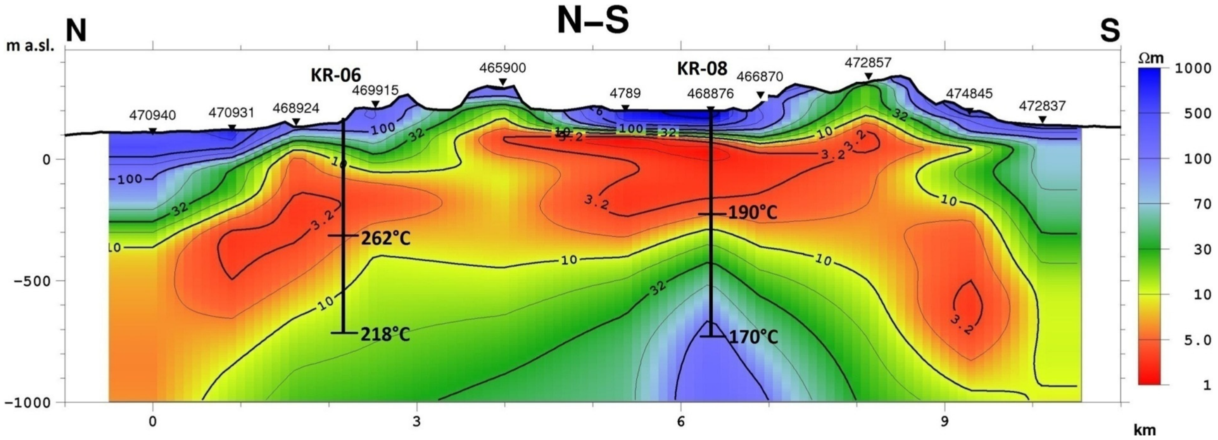

FIGURE 28: TEM resistivity cross-section along the profile down to 1000 m b.s.l., also showing temperature in drillholes KR-06 and KR-08

KR-06: This drillhole is 843 m deep. The conductive structure which is correlated with the smectite-zeolite and mixed layered clay zone extends from 50 m to a depth of 450 m. The highest measured drillhole temperature is at 500 m depth and is equal to 262°C (Figure 28). This measured value is rather high for the smectite-zeolite and mixed layered clay zone (Figure 25), as it is typical for the resistive chlorite-epidote zone which is indicative of temperature above 240°C. The measured bottom hole temperatures are found to be less than 220°C, which also does not conform to the chlorite-epidote seen there. These deviations show in the first place that in the uppermost part of the drillhole (at least down to 500 m) the alteration is lagging behind the rock temperature and in the second place that the geothermal system below 500 m is most likely cooling down and is not in equilibrium. In a geothermal system, when cooling happens, alteration and resistivity remain stable.

KR-08: This drillhole is 933 m deep with the smectite-zeolite zone extending from 200 to 400 m and the mixed-layered clay zone from 300 down to 700 m; the measured temperature down to 400 m is 190°C, which is in agreement with the alteration. However, the measured temperature at the bottom of the drillhole was only found to be 170°C, in the chlorite-epidote zone. This is also an indication that the geothermal system is presumably cooling down.

6. CONCLUSIONS

The resistivity cross-sections from the TEM and from 1-D joint inversion of MT and TEM data show three major resistivity structures. The high-resistivity uppermost layers of resistivity >70 Ωm are interpreted as unaltered basaltic dry lavas and hyaloclastites. The conductive cap (<10 Ωm) is associated with a smectite-zeolite or mixed layered clay zone followed by resistive layers, corresponding to the chlorite-epidote zone. Generally, a good correlation is found between the subsurface resistivity structure and alteration mineralogy of the Krýsuvík high-temperature area.

The measured temperatures for the two drillholes, KR-06 and KR-08, were analysed and compared with alteration mineralogy. In the chlorite-epidote zone, expected temperature values are above 240°C; however, here the measured temperature was less than 170°C for KR-08 and 218°C for KR-06. The discrepancy between the measured and the expected values show that parts of the geothermal system are probably cooling down. The resistivity values in this part of the geothermal reservoir cannot reflect temperature because the hydrothermal alteration and the rock temperature are not in equilibrium.

The 1-D joint inversion of MT and TEM data is a powerful method in mapping shallow to deep resistivity structures. Joint inversion is helpful in correcting static shift caused by near surface inhomogeneities.

ACKNOWLEDGEMENTS

It is my pleasure to thank the United Nations University Geothermal Training Programme and the Government of Iceland for sponsoring me to participate in this specialized training. Special gratitude goes to the director of UNU-GTP, Dr. Ingvar B. Fridleifsson and the deputy director, Mr. Lúdvík S. Georgsson for offering me the opportunity to participate in the Geothermal Training Program. Thanks to all staff members of UNU-GTP for their guidance and support.

Special thanks to my advisors Mr. Gylfi Páll Hersir and Mr. Knútur Árnason for their valuable time, special lectures and guidance. I would also like to thank Dr. Hjálmar Eysteinsson for his great support. All lecturers, Orkustofnun and ISOR staff members are greatly acknowledged for sharing their knowledge and experience. I am also grateful to the Geological Survey of Ethiopia for supporting my studies in Iceland.

Finally, I would like to thank the Almighty God for all his help.

REFERENCES

Abdelghafoor, M., 2007: Geological and geothermal mapping in Sveifluháls area, SW-Iceland. Report 3 in: *Geothermal Training in Iceland 2007*. UNU-GTP, Iceland, 1-23.

Archie, G.E., 1942: The electrical resistivity log as an aid in determining some reservoir characteristics. *Tran. AIME, 146,* 54-67.

Ármannsson, H., Kristmannsdóttir, H., Torfason, H., and Ólafsson, M., 2000: Natural changes in unexploited high-temperature geothermal areas in Iceland. *Proceedings of the World Geothermal Congress 2000, Kyushu-Tohuku, Japan*, 521-526.

Árnason, K., 1989: *Central loop transient electromagnetic sounding over a horizontally layered earth*. Orkustofnun, Reykjavík, report OS-89032/JHD-06, 129 pp.

Árnason, K., 2006a: *TEMTD. A program for 1D inversion of central-loop TEM and MT data. A short Manual.* ÍSOR, Reykjavík, 16 pp.

Árnason, K., 2006b: *TemX. A graphically interactive program for processing central-loop TEM data. A short manual.* ÍSOR, Reykjavík, 10 pp.

Árnason K., Eysteinsson, H., Hersir G.P., 2010: Joint 1D inversion of TEM and MT data and 3D inversion of MT data in the Hengill area, SW Iceland. *Geothermics, 39*, 13–34.

Arnórsson, S., Gudmundsson, G., Sigurmundsson, S.G., Björnsson, A., Gunnlaugsson, E., Gíslason, G., Jónsson, J., Einarsson, P., and Björnsson, S., 1975: *Krýsuvík. A general report on the geothermal exploration.* Orkustofnun, Reykjavík, report OS-JHD-7554 (in Icelandic), 71 pp.

Árnason, K., Karlsdóttir, R., Eysteinsson, H., Flóvenz, Ó.G., and Gudlaugsson, S.Th., 2000: The resistivity structure of high-temperature geothermal systems in Iceland. *Proceedings of the World Geothermal Congress 2000*, *Kyushu-Tohoku, Japan,* 923-928.

Cagniard, L., 1953: Basic theory of the magneto-telluric method of geophysical prospecting. *Geophysics, 18,* 605-635.

Dakhnov, V.N., 1962: Geophysical well logging. *Q. Colorado Sch. Mines, 57-2*, 445 pp.

Eysteinsson, H., 2010: *The resistivity plot programs, TEMMAP, TEMRESD and TEMCROSS.* ÍSOR, Reykjavík, unpublished manuals.

Eysteinsson, H., 1999: *Resistivity soundings around Sandfell, Reykjanes Peninsula*. Orkustofnun, report OS-99002 (in Icelandic), 71 pp.

Eysteinsson, H., 2001: *Resistivity soundings around Trölladyngja and Núpshlídarháls, Reykjanes Peninsula.* Orkustofnun, report OS-2001/038 (in Icelandic), 110 pp.

Flóvenz, Ó.G., Georgsson, L.S., and Árnason, K., 1985: Resistivity structure of the upper crust in Iceland. *J. Geophys. Res., 90-B12,* 10,136-10,150.

Flóvenz, Ó.G., Spangenberg, E., Kulenkampff, J., Árnason, K., Karlsdóttir, R., and Huenges E., 2005: The role of electrical conduction in geothermal exploration. *Proceedings of the World Geothermal Congress 2005, Antalya, Turkey, CD,* 9 pp.

Hersir, G.P., and Björnsson, A., 1991: *Geophysical exploration for geothermal resources. Principles and application*. UNU-GTP, Iceland, report 15, 94 pp.

Hersir, G.P., and Árnason, K., 2009: Resistivity of rocks. *Paper presented at "Short Course on Surface Exploration for Geothermal Resources", organized by UNU-GTP and LaGeo, Santa Tecla, El Salvador,* 8 pp.

Hersir, G.P., Vilhjálmsson, A.M., Rosenkjær, G.K., Eysteinsson, H., and Karlsdóttir, R., 2010: *The Krýsuvík geothermal field. Resistivity soundings 2007 and 2008.* ÍSOR - Iceland GeoSurvey, Reykjavík, report ÍSOR-2010/025 (in Icelandic), 263 pp.

ISL, Michigan State University, 1999: Liquid molding. ISL, Michigan State University, webpage islnotes.cps.msu.edu/trp/rtm/modl_mes.html.

Jones, A.G., 1988: Static shift of magnetotelluric data and its removal in a sedimentary basin environment. *Geophysics, 53-7,* 967-978.

Keller, G.V., and Frischknecht, F.C., 1966: *Electrical methods in geophysical prospecting.* Pergamon Press Ltd., Oxford, 527 pp.

Lemma D., Y., 2010: *Multidimensional inversion of MT data from Krýsuvík high-temperature geothermal field, SW Iceland, and study of how 1D and 2D inversion can reproduce a given 2D/3D resistivity structure using synthetic MT data.* University of Iceland, M.Sc. thesis, UNU-GTP, Iceland, report 4, 94 pp.

Manzella, A., 2007: *Geophysical methods in geothermal exploration.* Italian National Research Council, International Institute for Geothermal Research, Pisa, webpage: http://cabierta.uchile.cl/revista/12/articulos/pdf/A_Manzella.pdf, 40 pp.

Phoenix Geophysics, 2009: *Data processing. User's guide.* Phoenix Geophysics, Ltd., Toronto.

Quist, A.S., and Marshall, W.L., 1968: Electrical conductances of aqueous sodium chloride solutions from 0 to 800°C and at pressures to 4000 bars. *J. Phys. Chem., 72,* 684-703.

Rowland, B.F., 2002: *Time-domain electromagnetic exploration.* Northwest Geophysical Associates, Inc., 6 pp.

Simpson, F., and Bahr, K., 2005: *Practical magnetotellurics.* Cambridge University Press, Cambridge, UK, 254 pp.

SOHO, 2010: *Solar wind.* Solar and Heliospheric Observatory, internet website: *http://sohowww.nascom.nasa.gov/gallery/images/magfield.html.*

Sternberg, B.K., Washburn, J.C., and Pellerin, L., 1988: Correction for the static shift in magnetotellurics using transient electromagnetic soundings. *Geophysics, 53-11,* 1459-1468.

Vozoff, K., 1991: The magnetotelluric method. In: Nabighian, M.N (ed), *Electromagnetic methods in applied geophysics*, *2*, 641-711.

Ward, S.H, and Wannamaker, P.E., 1983: *The MT/AMT electromagnetic method in geothermal exploration*. UNU-GTP, Iceland, report 5, 107 pp.

APPENDIX I: TEM 1-D inversion models

The measured TEM data curve is shown with red (dark) dots; the calculated TEM data curve is a black line connecting the red (dark) dots, and the 1-D layered modelling is in green (gray).

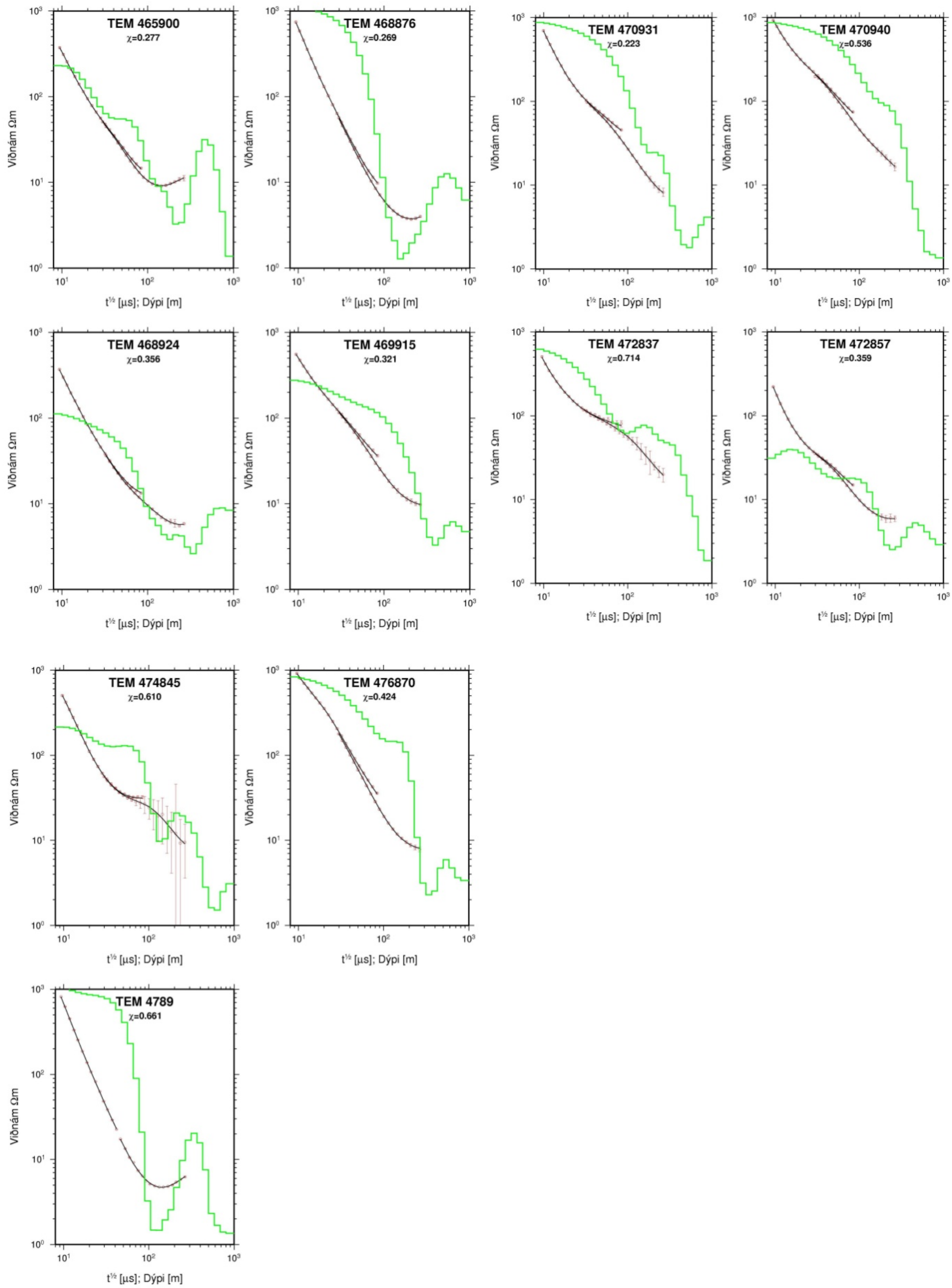

APPENDIX II: MT data (EDI)

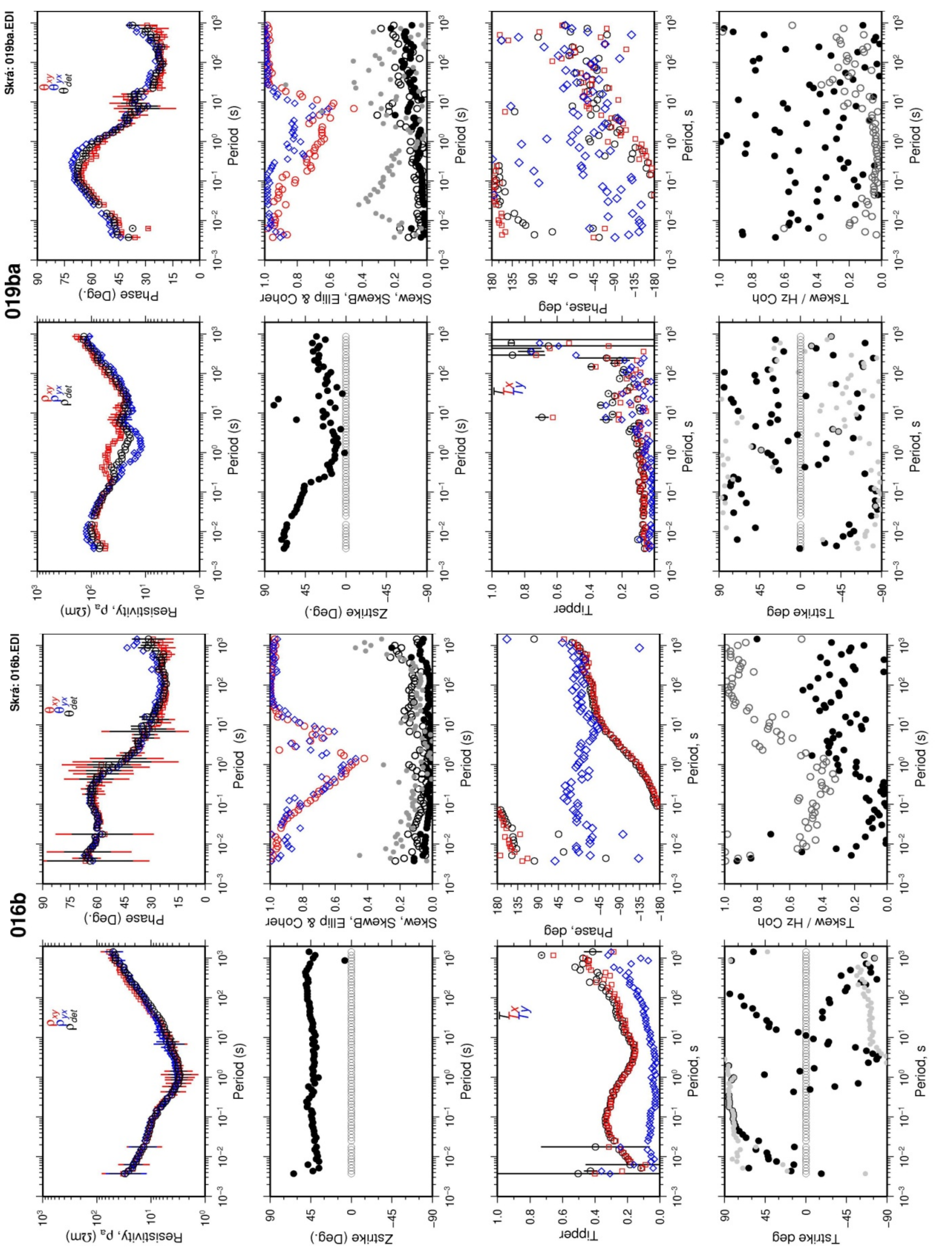

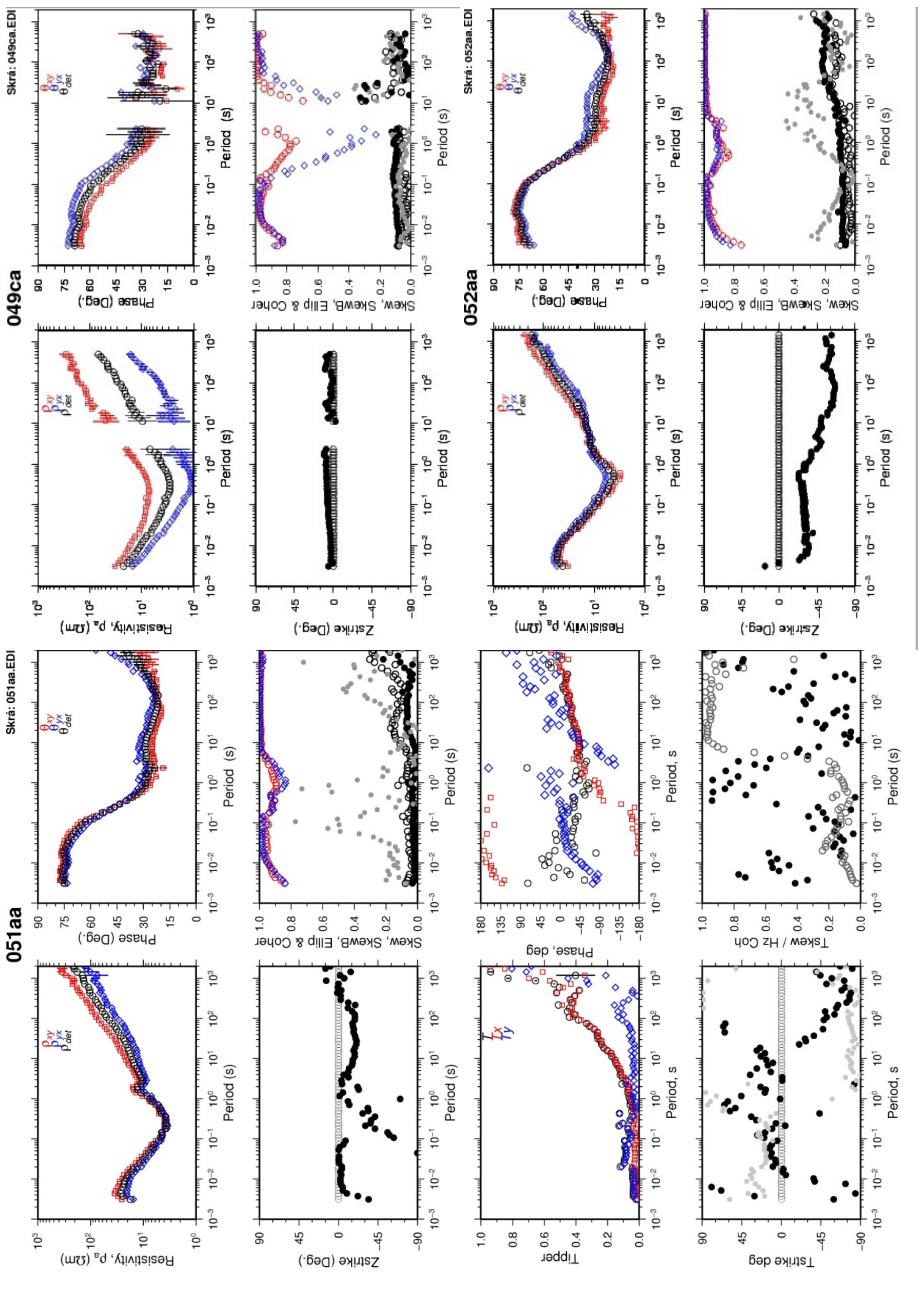
051aa
Skrá: 051aa.EDI
049ca
Skrá: 049ca.EDI
052aa
Skrá: 052aa.EDI

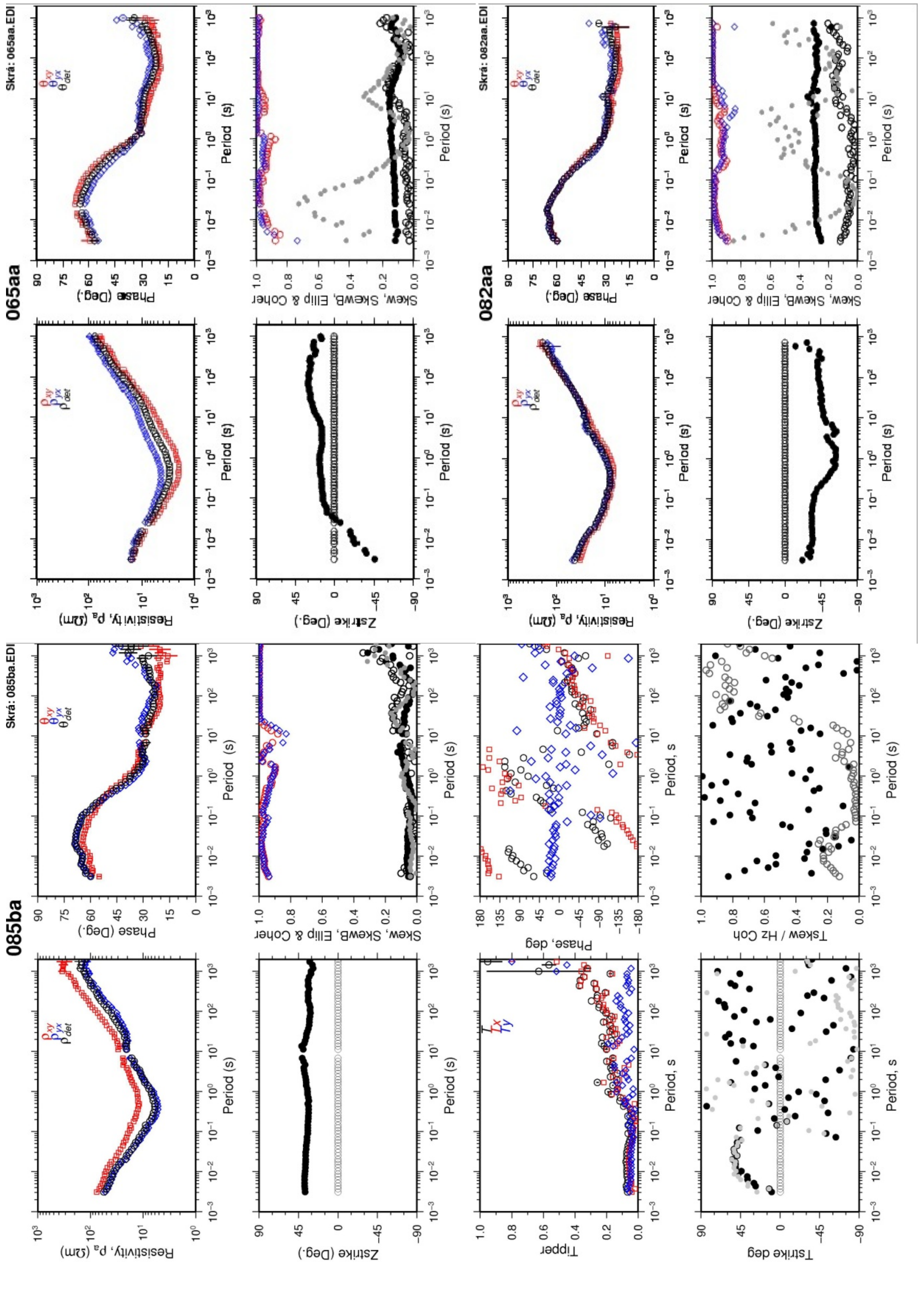
085ba
Skrá: 085ba.EDI
065aa
Skrá: 065aa.EDI
082aa
Skrá: 082aa.EDI

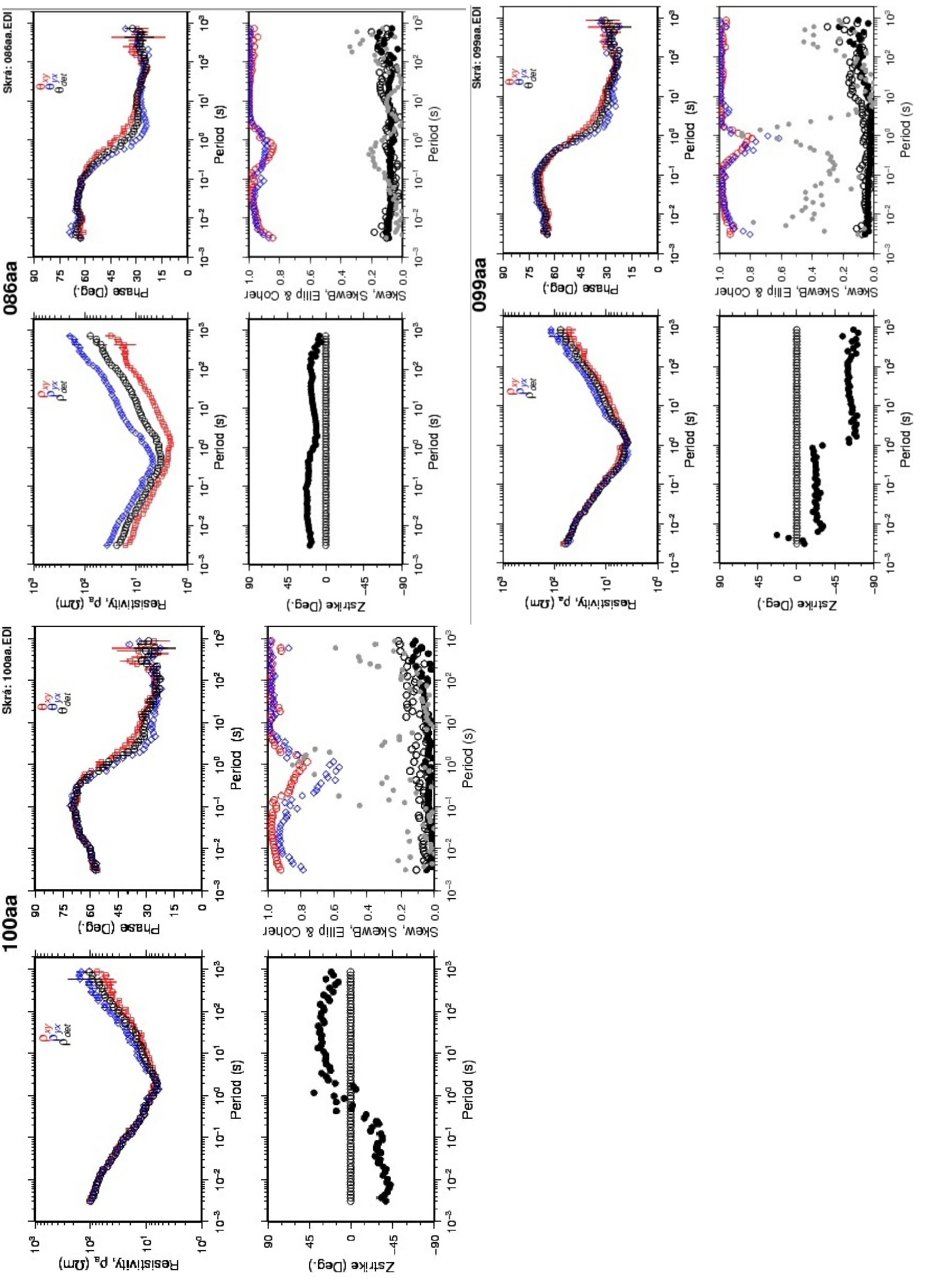

100aa
Skrá: 100aa.EDI
086aa
Skrá: 086aa.EDI
099aa
Skrá: 099aa.EDI
Resistivity, ρa (Ωm)
Phase (Deg.)
Zstrike (Deg.)
Skew, SkewB, Ellip & Coher
Period (s)

APPENDIX III: TEMTD 1-D TEM and MT joint inversion models

The red (dark) line represents the TEM curve and blue (gray) represents the MT curve. The green (gray) line to the right represents 1-D layered resistivity modelling.

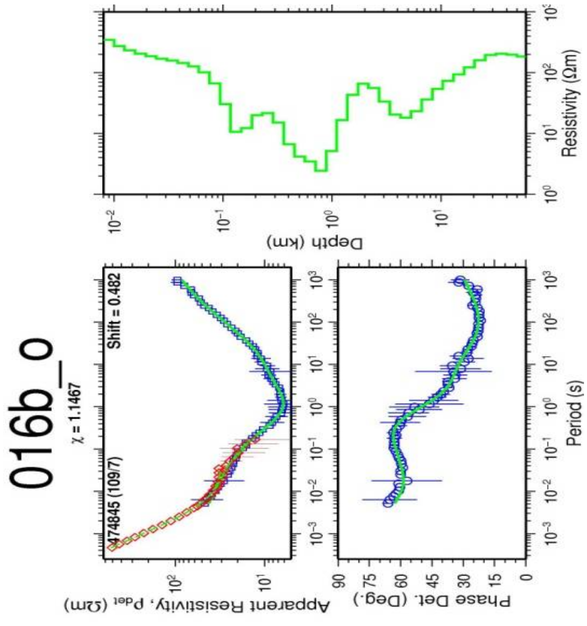

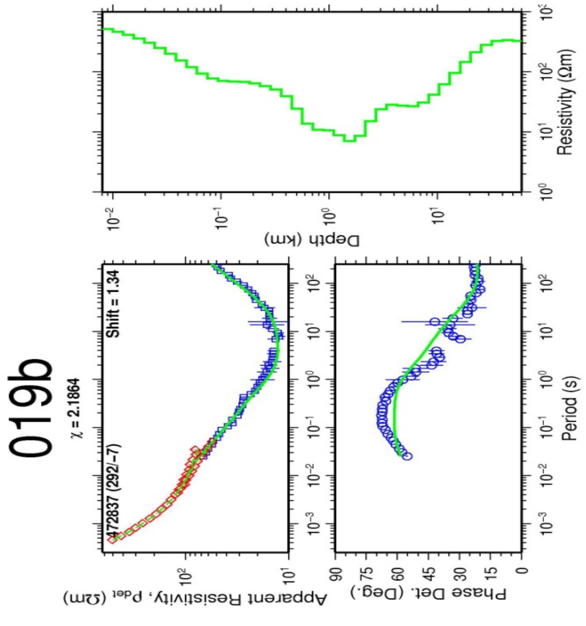

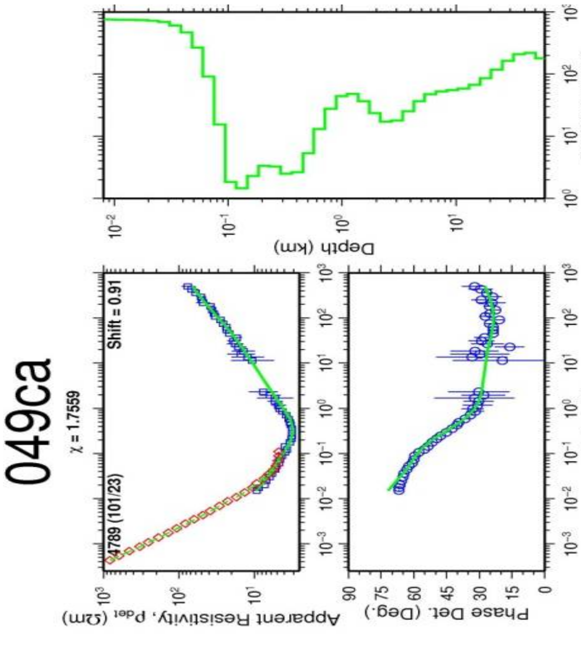

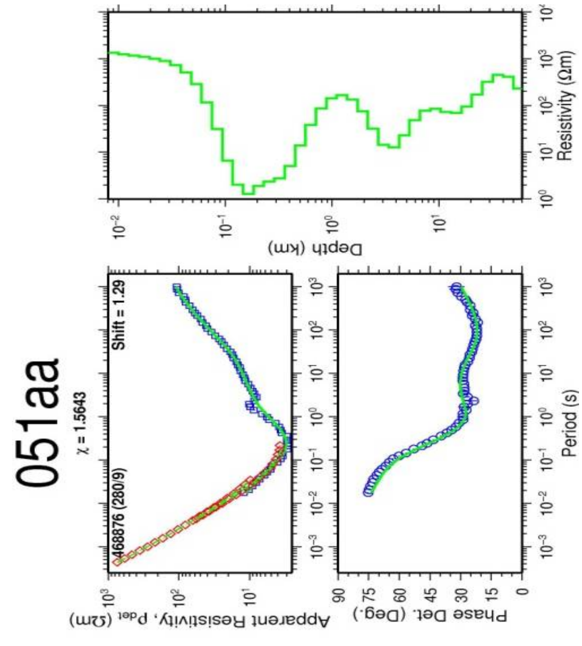

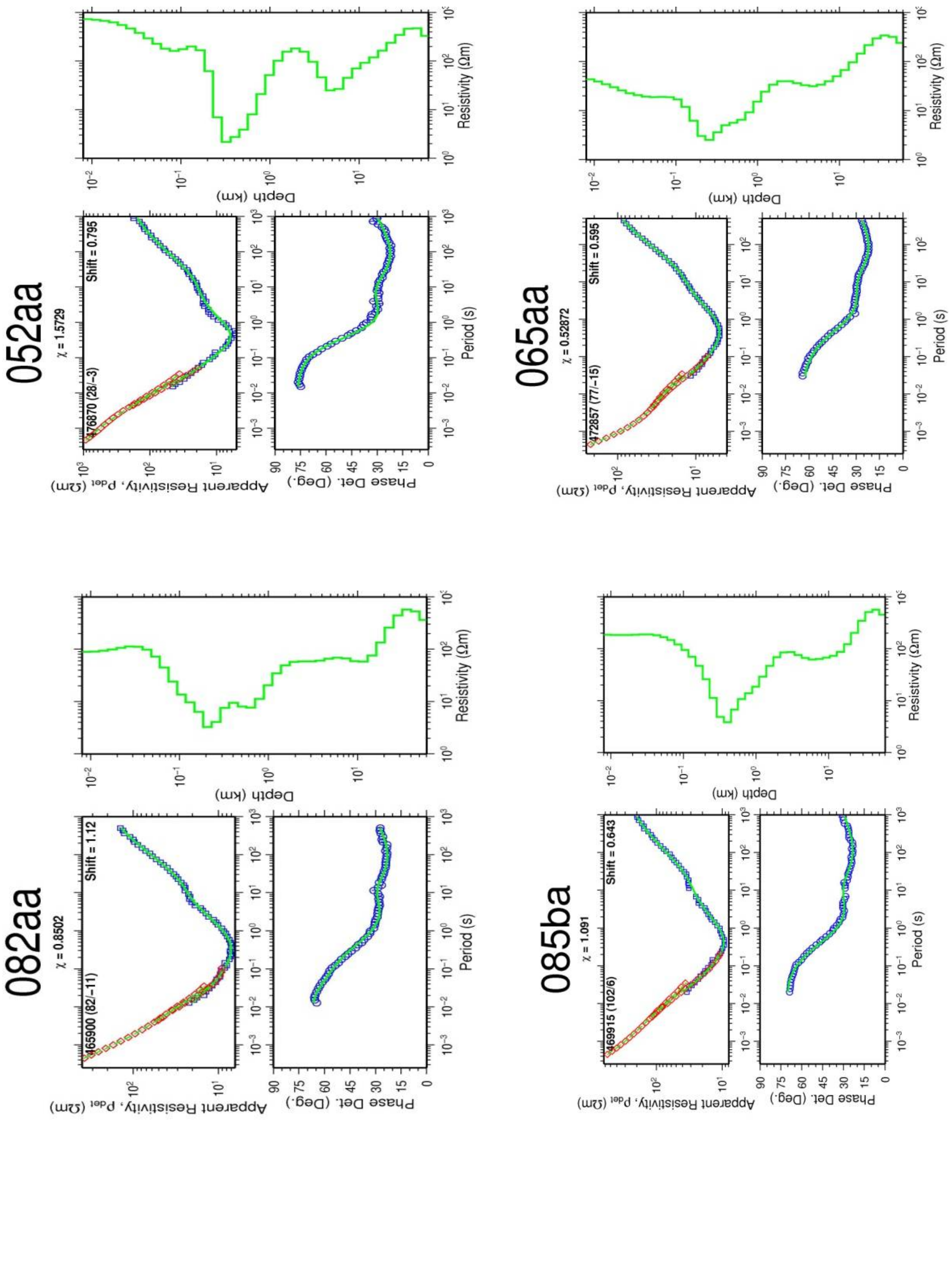
082aa
χ = 0.8502
465900 (82/-11)
Shift = 1.12
052aa
χ = 1.5729
476870 (28/-3)
Shift = 0.795
085ba
χ = 1.091
469915 (102/6)
Shift = 0.643
065aa
χ = 0.52872
472857 (77/-15)
Shift = 0.595
Apparent Resistivity, ρdet (Ωm)
Phase Det. (Deg.)
Period (s)
Depth (km)
Resistivity (Ωm)

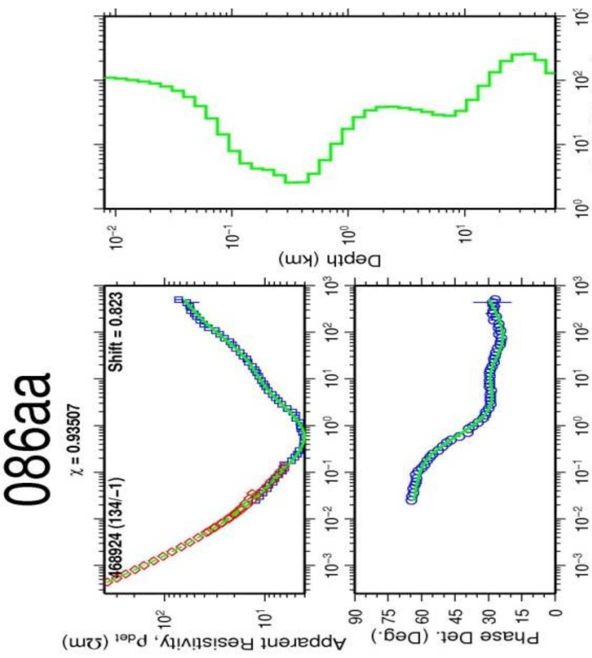
086aa
χ = 0.93507
468924 (134/−1)
Shift = 0.823
Apparent Resistivity, ρdet (Ωm)
Phase Det. (Deg.)
Period (s)
Depth (km)
Resistivity (Ωm)

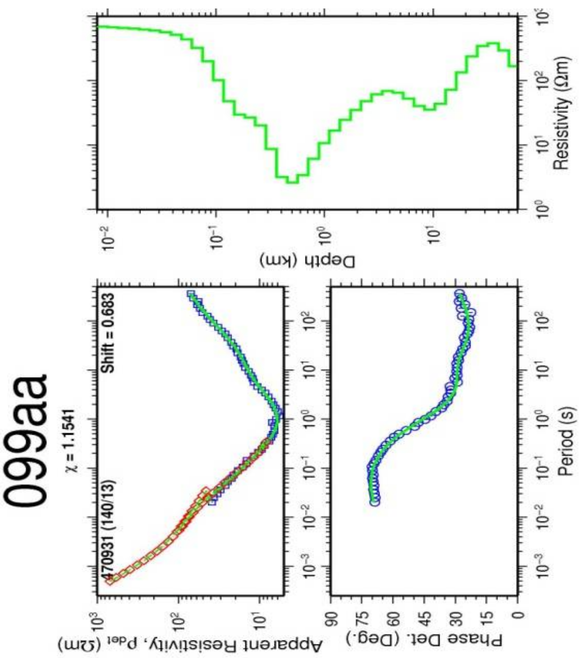
099aa
χ = 1.1541
470931 (140/13)
Shift = 0.683
Apparent Resistivity, ρdet (Ωm)
Phase Det. (Deg.)
Period (s)
Depth (km)
Resistivity (Ωm)

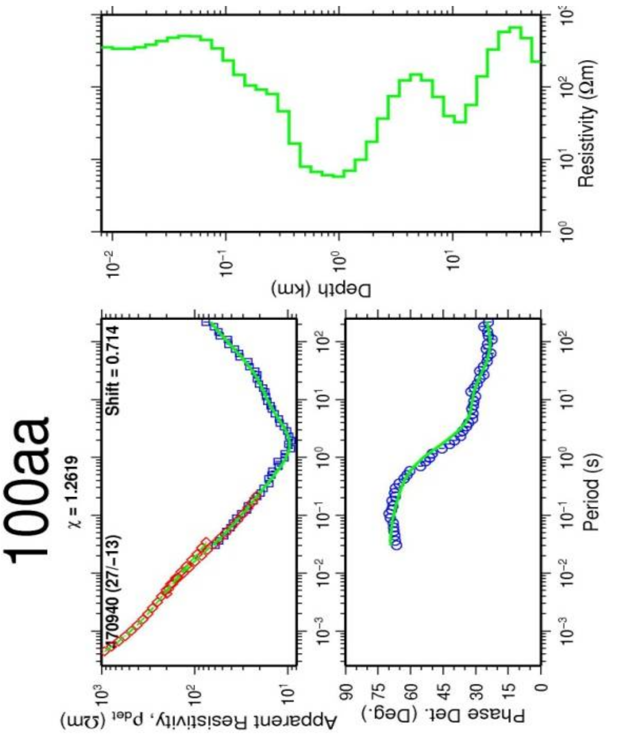
100aa
χ = 1.2619
470940 (27/−13)
Shift = 0.714
Apparent Resistivity, ρdet (Ωm)
Phase Det. (Deg.)
Period (s)
Depth (km)
Resistivity (Ωm)